Graphical Abstract (for review)

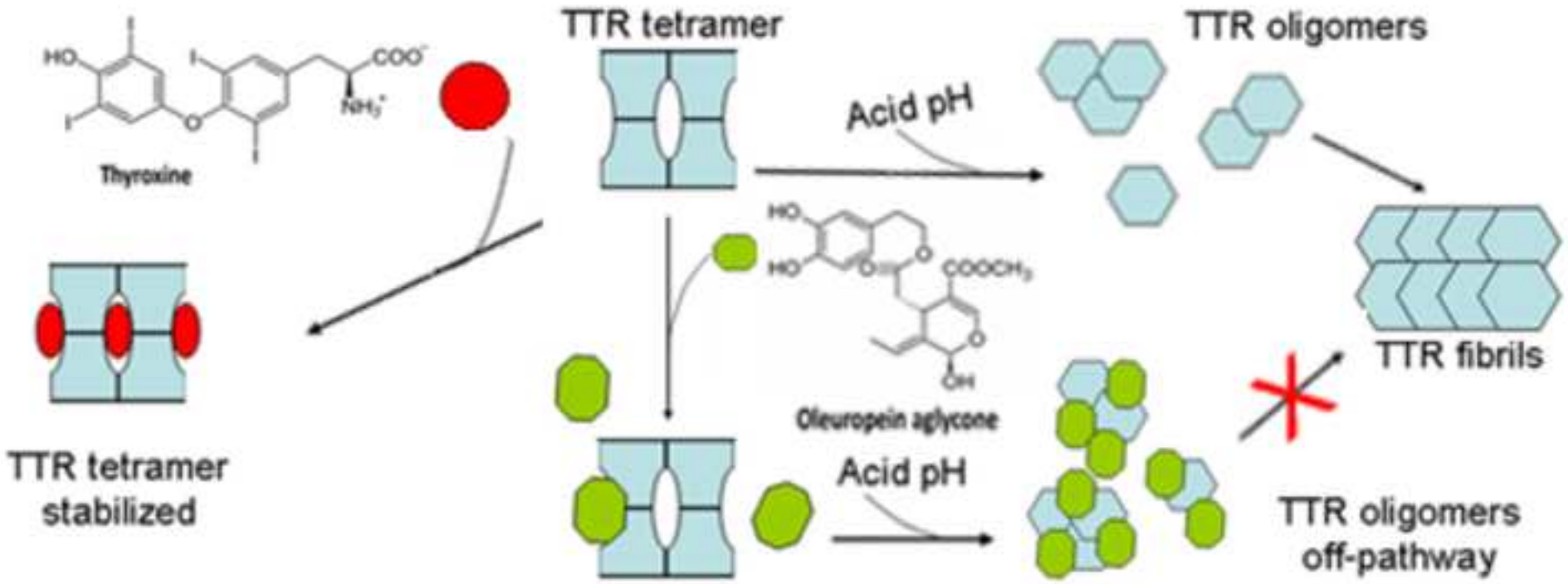

Highlights:

- Oleuropein aglycone inhibits toxic aggregation of wild type and L55P Transthyretin
- Oleuropein aglycone reduces the membrane/transthyretin interaction
- Oleuropein aglycone remodels and degrades wt-TTR and L55P amyloid fibrils
- Oleuropein aglycone might be used to hinder TTR- related pathologies

The Polyphenol Oleuropein aglycone hinders the growth of toxic Transthyretin amyloid assemblies

Manuela Leri[1#], Daniele Nosi[2#], Antonino Natalello[3], Riccardo Porcari[5] , Matteo Ramazzotti[1], Fabrizio Chiti[1,7], Vittorio Bellotti[5,6], Silvia Maria Doglia[3,4], Massimo Stefani[1,7], Monica Bucciantini[1,7*]

[1] Dipartimento di Scienze Biomediche Sperimentali e Clinche "Mario Serio"- Università degli Studi di Firenze, Viale Morgagni 50, 50134 Firenze, Italy. manuela.leri@unifi.it; matteo.ramazzotti@unifi.it; fabrizio.chiti@unifi.it; massimo.stefani@unifi.it.

[2] Dipartimento di Medicina Sperimentale e Clinica - Università degli Studi di Firenze, Largo Brambilla 3, 50134 Firenze, Italy. daniele.nosi@unifi.it.

[3] Dipartimento di Biotecnologie e Bioscienze, Università di Milano-Bicocca, Piazza della Scienza 2, 20126 Milano, Italy antonino.natalello@unimib.it;

[4] Dipartimento di Fisica G. Occhialini, Università degli Studi di Milano-Bicocca, Piazza della Scienza 3, 20126 Milano, Italy silviamaria.doglia@unimib.it.

[5] Wolfson Drug Discovery Unit, Centre for Amyloidosis and Acute Phase Proteins, Division of Medicine, Royal Free Campus University College London, NW3 2PF London, UK r.porcari@ucl.ac.uk; v.bellotti@ucl.ac.uk

[6] Dipartimento di Medicina Molecolare – Istituto di Biochimica – Università degli Studi di Pavia, 27100 Pavia, Italy.

[7] Centro Interuniversitario per lo Studio delle Malattie Neurodegenerative (CIMN), 50134 Firenze, Italy

[#] Equal contribution

[*] To whom correspondence should be addressed

Monica Bucciantini, monica.bucciantini@unifi.it, Dipartimento di Scienze Biomediche Sperimentali e Clinche "Mario Serio"- Università degli Studi di Firenze, viale Morgagni 50, 50134 Firenze, Italy

Running Title: Oleuropein hinders TTR aggregation

Abstract

Transthyretin (TTR) is involved in a subset of familial or sporadic amyloid diseases including senile systemic amyloidosis (SSA), familial amyloid polyneuropathy and cardiomyopathy (FAP/FAC) for which no effective therapy has been found yet. These conditions are characterized by extracellular deposits primarily found in the heart parenchyma and in peripheral nerves whose main component are amyloid fibrils, presently considered the main culprits of cell sufferance. The latter are polymeric assemblies grown from misfolded TTR, either wt or carrying one out of many identified mutations. The recent introduction in the clinical practice of synthetic TTR-stabilizing molecules that reduce protein aggregation provides the rationale to search natural effective molecules able to interfere with TTR amyloid aggregation by hindering the appearance of toxic species or by favoring the growth of harmless aggregates. Here we carried out an in depth biophysical and morphological study on the molecular features of the aggregation of wt- and L55P-TTR involved in SSA or FAP/FAC, respectively, and on the interference with fibril aggregation, stability and toxicity to cardiac HL-1 cells of demonstrate the ability of Oleuropein aglycone (Ole*A*), the main phenolic component of the extra virgin olive oil. We describe the molecular basis of, such interference and of the resulting reduction to inhibit of TTR amyloid aggregate cytotoxicity. Our data offer the possibility to validate and optimize the use of Ole*A* or its molecular scaffold to rationally design promising drugs against TTR-related pathologies that could enter a clinical experimental phase.

Keywords: Transthyretin; Oleuropein Aglycone; Amyloid; FAP; FAC

Abbreviations: TTR, Transthyretin; SSA, Senile systemic amyloidosis; FAP, Familial amyloid polyneuropathy; FAC, Familial amyloid cardiomyopathy; wt-TTR, wild-type TTR; OleA, Oleuropein aglycone; NDGA, nordihydroguaiaretic acid; EGCG, epigallocatechin 3-gallate; DMSO, dimethylsulfoxide; CR, Congo Red; TEM, trasmission electron microscope; FBS, fetal bovine serum; DLS: Dinamic Light scattering; MTT, 3-(4,5-dimethylthiazol-2-yl)-2,5-diphenyltetrazolium bromide; CTX-B, Cholera enterotoxin subunit B; FTIR, Fourier transformed infrared; GM1, monosialotetrahexosylganglioside 1; FRET, Fluorescence Resonance Energy Transfer; Dh, hydrodynamic diameter; PBS, phosphate buffer saline; BSA, Bovine serum albumine; Trp, Tryptophane.

Chemical compounds: Oleuropein Aglycone (PubChem CID: 56842347); Dimethylsulfoxide (PubChem CID: 679); Congo Red (PubChem CID: 11313); MTT (PubChem CID: 64965); Acrylamide (PubChem CID: 6579); Sodium Dodecil Sulfate (PubChem CID: 3423265); N,N-dimethylformamide (PubChem CID: 6228).

1. Introduction

Human transthyretin (TTR) is a 55 kDa homotetrameric protein composed of 127-residue subunits [1] synthesized in the liver (90%), retinal epithelium, pancreas and choroid plexus [2] and present in the plasma at a 20-40 mg/ml concentration, with a 1-2 day residence time [2]. TTR transports in the blood and the cerebrospinal fluid about 15% of total thyroxine (T4) and the holo-retinol-binding protein [3]. TTR is a well known human amyloidogenic protein whose aggregates are involved in diseases including senile systemic amyloidosis (SSA), familial amyloid polyneuropathy (FAP) and cardiomyopathy (FAC) often resulting in severe outcomes [4]. SSA is a late onset sporadic disease affecting about 25% of individuals over 80 years in which wild-type TTR (wt-TTR) misfolds and aggregates into amyloid deposits preferentially found at the terminals of peripheral nerves and in the heart [5, 6]. FAP and FAC are early-onset pathologies associated to one out of a relevant number of mutations in the TTR gene (over 100 identified so far). In most cases, in these forms single amino acid substitutions result in misfolding of the tetramer and amyloid aggregation of the so-generated monomers/dimers, whose deposits are found in the peripheral and autonomic nervous system and in the heart [7].

Among the described TTR variants, the first identified and the most frequent is V30M [8], although one of the mutant TTR giving the most aggressive (and with the earliest onset) disease is L55P (L55P-TTR) [9]. Past studies on the molecular determinants of TTR misfolding and aggregation have led to relate the amyloidogenic potential of the TTR variants to the destabilization and dissociation of the tetrameric native state into misfolded or partially unfolded dimeric/monomeric species, whose reduced stability is largely contributed by the increased exposure of hydrophobic surfaces [10]. Currently, TTR tetramer dissociation is recognized as the rate-limiting step of amyloid fibril nucleation and growth [11].

Without adequate therapy, TTR amyloidosis results in a fatal outcome, leading to death within 10-15 years mainly following heart complications. However, besides liver and heart transplantation, there is no effective medical treatment to enhance or to block disease progression. Accordingly, therapeutic strategies are mainly aimed at hindering tetramer dissociation and at inhibiting or modifying the resulting TTR aggregation. Preliminary results with molecules able to stabilize the native state of TTR and to hinder amyloid growth, suggest the possibility of a chemotherapeutic approach to treat TTR amyloidosis [12]. Encouraging results have emerged on the possible use in therapy of several TTR stabilizers such as tafamidis (the first disease-modifying pharmacotherapy to be approved for use in adult patients with early-stage TTR-FAP) and diflunisal, demonstrating the feasibility of this approach [12]; these results also suggest the opportunity to increase the number of potentially exploitable molecules by searching natural compounds able to interfere with amyloid aggregation either by stabilizing the TTR fold, by modifying the aggregation path so as to hinder the appearance of toxic species in the aggregation path and/or by favoring the growth of less toxic assemblies.

Recent research has highlighted the beneficial effects of natural phenols, a class of compounds found in several foods of plant origin [13], in a number of amyloid diseases. In particular, it has repeatedly been reported that Mediterranean diet, enriched in polyphenolic compounds such as resveratrol (contained in red wine) and

Oleuropein aglycone (Ole*A*, the main polyphenol in the extra virgin olive oil) is effective against age-related damages and improves disease-associated behavioral deficits [14-16]. The beneficial effects of Ole*A* against amyloid toxicity to cultured cells [17-19] and in transgenic model organisms [20, 21] stems from several effects at the molecular and cellular level, the most important of which are related to the ability of Ole*A* to counteract *in vitro* the aggregation of proteins such as tau, amylin and Aβ42, effectively hampering the formation of toxic oligomeric species [17-19]. However, more knowledge must be provided on the effect of Ole*A* against aggregation and aggregate toxicity of many other amyloid-associated peptides and proteins, since the effect of polyphenols against protein misfolding and aggregation can result from different molecular mechanisms [22].

Some of the investigated natural polyphenols such as resveratrol, curcumin, nordihydroguaiaretic acid (NDGA) and epigallocatechin 3-gallate (EGCG) bear similarities with thyroxine (T4), the TTR physiological ligand that is known to stabilize the native tetrameric form of the protein [23]; accordingly, they have been investigated for their ability to stabilize the TTR tetramer, hindering its disassembly and the ensuing aggregation into toxic amyloid assemblies. These studies showed that all these compounds stabilize TTR or inhibit its toxic aggregation by three different mechanisms: (i) EGCG and resveratrol stabilize the TTR tetramer suppressing its dissociation into dimers/monomers and thereby the growth of cytotoxic species [23]; (ii) curcumin induces TTR oligomerizzation into a characteristic homogeneous population of "off-pathway" non-toxic small aggregates [24]; (iii.) NDGA reduces the amount of aggregated TTR [25]. Importantly, TTR oligomers and aggregation intermediates grown in the presence of EGCG and curcumin are not toxic to neuronal cells [23, 24].

In this study we extended previous data on the protection by natural polyphenols against TTR aggregation and cytotoxicity by investigating whether Ole*A* was able to interfere with the aggregation pathway and toxicity of both the wild-type protein and its L55P mutant and, whenever appropriate, trying to disentangle the underlying molecular mechanism of toxicity. Experiments on cytotoxicity were carried out with the cardiac muscle cell line HL-1, that retains the biochemical and electrophysiological properties of tissue cardiomyocytes [26]. We found that aggregation of wt-TTR and its highly amyloidogenic L55P variant in the presence of Ole*A* results in the growth of substantially harmless assemblies. Our data suggest a possible use of Ole*A* to treat TTR-related pathologies with the aim to relieve or to delay the occurrence of the most severe cardiac symptoms.

2. Materials and Methods

2.1. Oleuropein deglycosylation

Oleuropein was purchased from Extrasynthese and deglycosilated by treatment with almond β-glycosidase (EC 3.2.1.21, Fluka, Sigma-Aldrich) as previously described [17]. Briefly, a 10 mM solution of Oleuropein in 310 µl of 0.1 M sodium phosphate buffer, pH 7.0, was incubated with 8.9 I.U. of β-glycosidase overnight at room temperature. The reaction mixture was centrifuged at 18000 rpm for 10 min to precipitate Oleuropein aglycone (Ole*A*), which was eventually resuspended in DMSO (dimethylsulfoxide) in stocks at 100 mM concentration. The complete Oleuropein deglycosylation was confirmed by assaying the glucose released in the supernatant

with the Glucose (HK) Assay kit (Sigma-Aldrich). Stocks of Ole*A* were kept frozen and protected from light, and were used within the same day once opened.

2.2. TTR samples

Recombinant wt- and L55P-TTR were expressed and purified according to Mangione et al. [27]. Lyophilized TTR was dissolved at 1.6 mM in 30 mM sodium phosphate buffer, pH 7.0 and its aggregation was primed by adding 100 mM sodium acetate buffer, pH 4.0. TTR fibrils were grown by incubating wt-TTR at 37 °C and pH 4.0 for 72 h whereas the L55P fibrils were grown upon incubation at 37 °C and pH 5.0 for 96 h, as previously reported [28]. Aggregation kinetics were followed by FTIR. In order to study the interference of Ole*A* with the aggregation process, wt-TTR and L55P-TTR were incubated with an excess (3X of Ole*A* for 72 h and 96 h, respectively; disaggregation experiments were carried out using pre-formed fibrils incubated with Ole*A* for different times.

2.3. Congo Red Assay

The assay was performed as previously described [29] taking into account that amyloid binding induces a characteristic shift from 490 nm to 540 nm in Congo Red (CR) maximal optical absorbance [30]. In particular, TTR (7.14 μM) aggregation was monitored in the presence or in the absence of 3 × Ole*A*. The disaggregation experiments were carried out by exposing pre-formed TTR fibrils to Ole*A* for 10 min or 5 h. Both native, tetrameric wt-TTR and TTR fibrils were incubated with 5.0 mM sodium phosphate buffer, pH 7.0 containing 150 mM NaCl and 20 μM CR. The CR spectra were recorded in the 400-700 nm region using a Jasco V-630 Spectrophotometer. Blank spectra were acquired for CR alone, in the presence or in the absence of Ole*A*, and subtracted to each sample spectrum.

2.4. Transmission Electron Microscopy

5.0 μl aliquots of the TTR kept at aggregation conditions and incubated in the presence or in the absence of 3 × Ole*A* were withdrawn at different time points, loaded onto a formvar/carbon-coated 400 mesh nickel grids (Agar Scientific, Stansted, UK) and negatively stained with 2.0% (w/v) uranyl acetate (Sigma-Aldrich). The grid was air-dried and examined using a JEM 1010 trasmission electron microscope (TEM) at 80 kV excitation voltage.

2.5. Isolation and culture of HL-1 cardiomyocytes

HL-1 mouse atrial myocytes were obtained from Dr W. C. Claycomb (Louisiana State University Health Science Center, New Orleans, LA, USA) and grown in T25, gelatin/fibronectin-coated flasks, as previously described [31]. The cells were maintained in Claycomb Medium (JRH Biosciences) supplemented with 10% fetal bovine serum (FBS) containing 2.0 mM L-glutamine, 0.1 mM noradrenaline and 100 U/mL penicillin-streptomycin (Sigma-Aldrich). Every three days the cells (70-90% confluent) were detached and re-plated at a 1:3 dilution in a new T25 flask or in 96 well plates and used for measurements.

2.6. MTT assay

Cell viability was assessed by the MTT assay optimized for the cell line used in the experiments. Briefly, HL-1 cells were seeded into 96-well plates at a density of 6000 cells/well in fresh complete medium and grown for 48 h. Then, the cells were treated for 24 h with 20 μM wt-TTR or L55P-TTR at different times of aggregation or

with pre-fibrillar aggregates in the presence or in the absence of 60 μM Ole*A*. After 24 h of incubation, the culture medium was removed and the cells were incubated for 1.0 h at 37 °C in 100 μl of serum-free DMEM without phenol red, containing 0.5 mg/ml MTT. Then, 100 μl of cell lysis solution (20% SDS, 50% N,N-dimethylformamide) was added to each well and the samples were incubated at 37 °C to allow complete cell lysis. The absorbance of the blue formazan resulting form reduction of MTT was read at 570 nm using a spectrophotometric microplate reader. The final absorption values were calculated by averaging each sample in triplicate and subtracting blank average (100 μl of MTT solution + 100 μl of lysis solution).

2.7. Confocal Immunofluorescence

Subconfluent HL-1 cells grown on glass coverslips were treated for 24 h with the different samples of wt-TTR or L55P-TTR (20 μM) and then washed with PBS. GM1 labeling was performed by incubating the cells with 10 ng/ml CTX-B Alexa488 in complete medium for 10 min at room temperature. Then the cells were fixed in 2.0% buffered paraformaldehyde for 10 min and permeabilized by treatment with a 50% acetone/50% ethanol solution for 4.0 min at room temperature, washed with PBS and blocked with PBS containing 0.5% BSA and 0.2% gelatin. After incubation for 1.0 h at room temperature with a rabbit anti-TTR polyclonal antibody diluted 1:600 in the blocking solution, the cells were washed with PBS for 30 min under stirring and then incubated with Alexa568-conjugated anti-rabbit secondary antibody (Molecular Probes) diluted 1:100 in PBS. Finally, the cells were washed twice in PBS and once in redistilled water to remove non-specifically bound antibodies. Cell fluorescence was imaged using a confocal Leica TCS SP5 scanning microscope (Leica, Mannheim, Ge) equipped with a HeNe/Ar laser source for fluorescence measurements. The observations were performed using a Leica Plan 7 Apo X63 oil immersion objective. FRET analysis was performed by adopting the FRET sensitized emission method as previously reported [32]. 3D volume renderings were obtained by using the OsiriX software [32].

2.8. Dynamic light scattering

Dynamic light scattering (DLS) measurements were performed in a low-volume quarz cuvette (Hellma Analytics, Müllheim, Germany) using a Zetasizer Nano S DLS device from Malvern Instruments (Malvern, Worcestershire, UK) thermostated at 37 °C with a Peltier system. Size distributions by intensity and total light-scattering intensity were determined in 10 acquisitions (cell position 4.2 cm, attenuator index 7) of 10 seconds each, over a period of 10 min. The reported data are the average of three independent measurements.

2.9. FTIR spectroscopy

Aliquots of lyophilized TTR samples were suspended at 80 μM final concentration in 30 mM deuterated phosphate buffer, with or without Ole*A*, at different pH values. Deuterated buffers containing Ole*A* were prepared from a stock solution of 50 mM Ole*A* in DMSO. Fourier transformed infrared (FTIR) spectra were collected and analyzed as previously described [33, 34]. In particular, 15 μl of protein solution was placed in a temperature-controlled transmission cell (Wilmad, USA) with BaF2 windows and an optical path made by a Teflon spacer of 100 μm. FTIR spectra were collected in transmission mode during incubation at 37 °C for 72-96 h in the transmission cell. A Varian 670-IR spectrometer (Varian Australia Pty Ltd., Mulgrave VIC, AU) was

used under the following conditions: 2.0 cm-1 spectral resolution, 25.0 KHz scan speed, triangular apodization, and 256-1000 scan co-additions. After 72-96 h at 37 °C, the same solution was heated up to 100 °C at a rate of 0.2 °C/min. The same characterizations were performed for either wt-TTR at pH 3.5 and L55P at pH 5.5 in the absence or in the presence of Ole*A*. The pH 3.5 was chosen to promote aggregation at 37 °C of a highly concentrated (80 μM) wt-TTR sample required for FTIR measurements in transmission mode. Resolutions-Pro software (Varian Australia Pty Ltd., Mulgrave VIC, AU) was used for spectra processing, including buffer subtraction, vapor correction (when necessary) and the second derivative analyses transformation [33-35].

2.10. Intrinsic fluorescence measurements

Spectra of wt-TTR and L55P-TTR intrinsic fluorescence were collected at 295 nm excitation wavelength before and after adding Ole*A* and the emission intensity was scanned in the 300-400 nm range. The fluorescence emission spectra were normalized to an intensity of 1.0 at the observed λ max using the FL WinLab software (Perkin-Elmer Instrument Corporation, Wellesley, MA) prior to derivatization. Normalization of aromatic residues emission scan was essential to compare the intensities and the positions of the various bands appearing in the second derivatives of the fluorescence emission scans. Five independent spectra were averaged, smoothed with a 11-point moving window average and a Savitzky-Golay algorithm and finally the second derivatives of the smoothed spectra were obtained using the Omnic-software (Nicolet Inc., Madison, WI) [36]. Such smoothing step was required to reduce the noise in the second derivative and designed to met two main criteria: (i) the overall shape and intensity of the raw emission scan was not affected by the smoothing and (ii) the overall shape of the bands in the second derivative was preserved.

2.11. Acrylamide Quenching

Aliquots of the protein solutions were withdrawn at various aggregation times, mixed with increasing acrylamide quenching concentrations (0 to 0.6 M) in 30 mM phosphate buffer, pH 7.0, and incubated for 5 min in the dark. The intrinsic fluorescence was recorded before and after addition of the quencher. The excitation wavelength was set at 295 nm and the emission intensity was scanned in the 300-450 nm range. Fluorescence intensities were corrected for dilution resulting from stepwise addition of acrylamide. Stern-Volmer plots for TTR were fitted with the equation $F0/F = (1 + K\text{sv-A}) \exp(K\text{st})\text{A})$, where $F0$ and F are the intrinsic fluorescence intensities in the absence and in the presence of acrylamide, respectively, A is the concentration of acrylamide, Ksv is the Stern-Volmer constant for dynamic quenching and Kst is the static component of the quenching process [37].

2.12. Statistical Analysis

Statistical analysis of the data was performed by using one way analysis of variance (ANOVA) and Bonferroni test to determine differences in cytotoxicity.

3. Results

Recent data with cultured cells, transgenic animal models and clinical trials indicate that Ole*A* exhibits a wide range of pharmacological properties (Fig. 1) and is protective against type 2 diabetes, non-alcoholic liver steatosis, atherosclerosis, age-associated neurodegeneration [38, 39], obesity [40] and cardiovascular diseases [41]. In the present study we investigated, for the firs time, whether Ole*A* was able to interfere with TTR aggregation and to protect mouse HL-1 cardiomyocyte cells against the cytotoxicity induced by previously grown amyloid aggregates of wt-TTR and L55P-TTR.

3.1. Ole*A* interferes with TTR aggregation

wt-TTR and L55P-TTR were incubated in 30 mM sodium phosphate buffer, pH 7.0, for 30 min at 37 °C in the presence of Ole*A* at a 1:3 monomeric TTR:Ole*A* molar ratio. Then, the pH of the aggregation medium was shifted to 4.0 (wt-TTR) or to 5.0 (L55P-TTR) to prime aggregation [42]. At different times, aliquots of aggregate solutions were withdrawn and analyzed by means of different spectroscopic techniques.

To investigate the structural basis of the relation between Ole*A* and TTR aggregation we first assessed whether the polyphenol was able to interfere with the aggregation process. Thus, we compared the CR absorption spectra of TTR samples at aggregation conditions in the presence or in the absence of Ole*A*. The maximum CR absorption in the presence of wt-TTR or L55P-TTR at pH 7.0 was found at ca. 490 nm, which corresponds to unbound CR (Fig. 2a and 2c). However, the absorption peak completely shifted to ca. 540 nm when wt-TTR was incubated at pH 4 for 72 h (the so-called and typical red-shift, Fig. 2a), indicating the formation of amyloid. A similar peak also appeared with L55P-TTR incubated at pH 5.0 for 96 h, although in this case a residual peak at 490 nm was still present (Fig. 2c). At these conditions, the presence of Ole*A* in the aggregation mixture of both wt-TTR and L55P-TTR induced only a very slight reduction of the CR red-shift, suggesting that the polyphenol is not able to counteract effectively TTR aggregation. On the contrary, a remarkable reduction in the CR red-shift was observed when preformed aggregates of wt-TTR or L55P-TTR grown in the absence of Ole*A* were incubated with Ole*A* for 5 h (Fig. 2b and 2d), suggesting fibril disaggregation and/or remodeling activity by this polyphenol, even though a competition between CR and Ole*A* for the same binding sites on TTR aggregates cannot be excluded.

In parallel, the same samples were also analyzed by DLS for particle size characterization and the resulting average apparent hydrodynamic diameter (D_h) was used for comparison. The D_h of Ole*A* alone in our measurement conditions was found to be 193 ± 10.03 nm (data not shown) suggesting a micellar organization. At pH 7.0 the wt-TTR sample contained particles with a D_h of 6.9 ± 0.2 nm (Fig. 2e), a value consistent with previous data relative to soluble, tetrameric TTR [43]. After 30 min of aggregation at pH 4, the D_h raised to about 1000 nm (data not shown) and further increased to 1180 ± 86.19 nm in the following 72 h of aggregation (Fig. 1e). However, the same sample grown in the presence of Ole*A* (wt-TTR/Ole*A*-*i*72h) contained a homogenous and stable population of particles with D_h 327 ± 49.14 nm, corresponding to TTR bulky aggregates (Fig. 2e). When we analyzed L55P-TTR at pH 7.0, we found a particle population of 6.6 ± 0.3 nm, again

corresponding to the soluble, native tetrameric protein (Fig. 2g). After 96 h aggregation at pH 5 (L55P-TTR-*i*96h) the D_h increased to 1300 ± 74.88 nm (Fig. 2g). At the same conditions, the presence of Ole*A* (L55P-TTR/Ole*A*-*i*96h) induced a significant reduction of particle size to a value of ca. 500 ± 52.89 nm (Fig. 2g). Overall, these data indicate that Ole*A* drastically interferes with the aggregation path *in vitro* of both wt-TTR and its amyloidogenic mutant L55P-TTR, leading to aggregated material substantially different from that obtained in non-treated controls.

We also checked whether Ole*A* displayed any disaggregation activity to preformed fibrils. To do this, we treated with Ole*A* samples of pre-formed fibrils of both proteins for 10 min or 5 h (wt-TTR/Ole*A*-*dis*10m and wt-TTR/Ole*A*-*dis*5h; L55P-TTR/Ole*A*-dis10m and L55P-TTR Ole*A*-*dis*5h) and noticed a clear decrease in the apparent D_h values (Fig 2g and 2h), that were reduced from 141.77 ± 70 nm after 10 min to 68.06 ± 44.45 nm after 5 h for wt-TTR and from 105.71 ± 35 nm after 10 min to 43.821 ± 10 nm after 5 h for L55P-TTR. This finding suggests a disaggregating or remodeling effect of the polyphenol on TTR mature fibrils, confirming the data obtained with the CR analysis.

A deeper molecular investigation of the effect of Ole*A* on TTR secondary structures and aggregation was also carried out using FTIR spectroscopy. To disclose the different Amide I components, the second derivative of the FTIR absorption spectra are presented, where the minima correspond to the absorption maxima. Figs. 3a and 3g show the second derivative spectra of wt-TTR and L55P-TTR at pH 7.0, recorded at different times during sample incubation at 37 °C for 72 h or 96 h. The spectra at pH 7 for both proteins were found to be dominated by a component at 1628 cm^{-1}, which can be assigned to the native β-sheet structures of the proteins, in agreement with previous FTIR studies [44, 45]. In addition, a second β-sheet peak at around 1689 cm-1 was observed together with additional components ascribable to other elements of secondary structure (Fig. 3a, 3g) [33, 44]. The FTIR analysis after 72 h incubation of wt-TTR revealed only minor spectral changes (Fig. 3a), which resulted from the H/D exchange of the native protein [34]. On the contrary, at these conditions the L55P mutant displayed partial unfolding, as indicated by the decrease of the signal at 1628 cm-1 (Fig. 3g). Then, in order to better characterize the structural changes, we heated the samples within the IR cell up to 100 °C at a rate of 0.2 °C/min and collected each spectrum at 1.7 °C intervals. The recorded spectra indicated that wt-TTR, but not L55P-TTR, displays a very high thermal stability (Fig. 3b, 3h), in agreement with previous findings [44]. Indeed, at 100 °C wt-TTR retained about 50% of the initial intensity of the 1628 cm-1 peak (native β-sheets), whereas in the L55P-TTR this component was lost. Nevertheless, the increase in temperature allowed to observe in both wt-TTR and L55P-TTR the appearance and the proportional growth of a new peak at around 1615 cm^{-1} (typical of intermolecular β-sheets in protein aggregates [34, 45 44]), which was remarkably more intense in the mutant and persisted after sample cooling from 100 °C to 37 °C (Fig. 2b and 2h). These data indicate that at pH 7.0 and high temperature, unfolding and aggregation do initiate, even though more heavily in the mutant, and are not reversible.

The same study was also carried out for wt-TTR and L55P-TTR during aggregation at acid pH in the absence or in the presence of Ole*A* (Fig. 3c,d, 3e,f, 3i,l, and 3 m,n). The FTIR second derivative spectra recorded at

different times of acidic incubation showed several spectral changes both in wt- and in mutant TTR, which indicated a loss of native secondary structure and consequent protein aggregation (Fig. 3c and 3i). This was also evident when Ole*A* was present in the aggregation medium (Fig. 3e and 3m). In particular, the intensity of the spectral component at 1628 cm-1 associated with the native β-sheet decreased whereas two bands appeared around 1615 cm-1 and 1682 cm-1, signatures of intermolecular □-sheet structures in protein aggregates (Fig. 3c,e and 3i,m). At these conditions, heating both wt-TTR- and L55P-TTR resulted in the complete disappearance of the native spectral components and in the sharp increase of signals in spectral regions of intermolecular b-sheet, indicating further aggregation. This process was evident both in the presence and in the absence of Ole*A* (Fig. 3d,f and 3l,n), indicating that the polyphenol was not able to counteract heath-induced misfolding and aggregation of TTR.

Taken together, the reported data suggest that Ole*A* induces some remodeling of the supramolecular structure of the growing aggregates. This implies a mechanism of action different from that merely ascribable to some stabilization of the protein native structure hindering misfolding and aggregation, as observed for other anti-amyloidogenic compounds [12, 23].

3.2. Ole*A* reduces aromatic residues exposure on TTR aggregates

The aggregation of wt-TTR and L55P-TTR in the presence or in the absence of Ole*A* was further investigated by recording at regular time intervals during the aggregation process the intrinsic fluorescence spectra upon excitation at 295 nm. We observed that the emission maximum of wt-TTR underwent a red shift when the protein was incubated at pH 4.0 (Fig. 4a), suggesting a change in the polarity of the environment surrounding protein aromatic residues (mainly Trp) during the ongoing aggregation process. Such red-shift was significantly reduced in the presence of Ole*A* (Fig 4b). In order to enhance the interpretation of the fluorescence signals, we recorded the spectra at the same times of aggregation in the presence or in the absence of the polyphenol and analyzed their second derivatives (Fig. 4d). After 72 h of aggregation in the absence of Ole*A*, two main peaks were observed at around 330 nm and 360 nm, which are associated to different polarities of the environment surrounding aromatic residues. The 330 nm peak, indicating a low polarity environment, was evident in the native protein but shifted about to 340 nm after 10 min of aggregation and then gradually decreased at later times reaching its minimum at 72 h of aggregation (Fig. 4d). Conversely, the 360 nm peak, indicating a more polar environment, started to increase with the onset of aggregation and was particularly evident in samples aggregated for 48 h and 72 h. The observed structural transition was found to be largely attenuated in the presence of Ole*A*, with a second derivative spectrum indicating only minor reduction of the 330 and 360 nm peak intensities that are typical of the native protein (Fig. 4d).

The emission spectra of L55P-TTR in the native state and during the aggregation process are also shown in Fig. 4 along with the spectra recorded in the presence of Ole*A*. The second derivative profile of the fluorescence spectrum of this mutant displayed two peaks at 323 and 348 nm that gradually decreased in intensity and that showed a less evident red-shift with respect to that observed for wt-TTR, suggesting that such mutation consistently alters the conformation of TTR aggregates, as previously reported [9]. In this case, the presence of

Ole*A* had negligible effects (Fig. 4g and 4g-i). Finally, we found a significant increase of the low polarity environment of the aromatic residues in preformed fibrils of wt-TTR (Fig. 4c-e) and, to much lesser extent, L55P-TTR (Fig. 4 h-l) treated with Ole*A* for 5 h .

Finally, to shed further light on the structural perturbations in the hydrophobic core of the wt-TTR and L55P-TTR during aggregation in the absence or in the presence of Ole*A*, we carried out further experiments to directly assess the exposure of Trp residues. The extent of quenching of Trp intrinsic fluorescence by acrylamide has been shown to provide insight into solvent accessibility of the Trp residues [46]. To perform such experiments, aliquots of the wt-TTR and L55P-TTR samples were withdrawn from the aggregation solutions in the presence or in the absence of Ole*A* at various incubation times and mixed with acrylamide, then their fluorescence spectra (after excitation at 295 nm) were recorded in the 300-450 nm range. We observed time-dependent changes of intrinsic fluorescence quenching (Fig. 5a and 5d). In particular, we found a significant increase of acrylamide quenching as far as aggregation proceeded, reaching the highest values after 48 h and 48/72 h of aggregation for wt-TTR and L55P-TTR, respectively. These changes can reasonably be ascribed to an increased availability to the quencher of Trp residues in meta-stable intermediate states of the aggregation process. In the presence of Ole*A*, the increase of acrylamide quenching was reduced, especially at 48 h and 72 h of aggregation, where the maximum effect was observed in the absence of Ole*A* (Fig. 5b and 5e). These data indicate that Ole*A* reduces solvent-exposure of tryptophan residues in the aggregates grown from both wt-TTR and L55P-TTR, further confirming protein stabilization by the polyphenol (although some bias due to a preferential interaction of Ole*A* with exposed Trp residues cannot be excluded). Finally, we found that treating both wt-TTR and L55P-TTR preformed fibrils with Ole*A* induced an increase of Trp quenching (Fig. 5c-f), suggesting that the effect of Ole*A* in stabilizing meta-stable intermediate states relies on the reduction of the overall surface hydrophobicity of the aggregates.

3.3. Morphological analysis of the aggregates

After having completed the biophysical analysis of TTR aggregation and the interference of Ole*A*, we further investigated the aggregation path of the assemblies populating the different steps of the fibrillogenic process in the absence or in the presence of Ole*A* by TEM imaging. After 72 h of incubation at pH 4.0, wt-TTR consisted predominantly of bundling fibrils (Fig. 6a), whereas the L55P variant incubated for 96 h at pH 5.0 did not show uniform fibrillar structures (Fig. 6b). By contrast, only disordered assemblies were detectable in the samples of both proteins aggregated at the same conditions in the presence of Ole*A* (Fig. 6c,d). These data lend further support to the idea that Ole*A* does not prevent TTR aggregation by itself but, rather, it is effective in counteracting mature fibrils growth, a behavior comparable with that previously shown with tau [19], amylin [17] and Abeta peptides [18].

The time-dependent fibril disaggregating effect of Ole*A* reported above was also investigated by TEM. We noticed that upon incubation for 10 min with Ole*A*, pre-formed mature wt-TTR fibrils (wt-TTR/Ole*A*-*dis*10m) lost their structural uniformity and released into the incubation medium oligomer-like entities which formed a uniform layer onto the formvar support (Fig. 6 e and insert 5). When fibril incubation with Ole*A* was extended to

5 h (wt-TTR/Ole*A*-*dis*5h) fibrils size appeared further reduced and the layer of oligomer-like structures displayed increased density (Fig. 6f and insert 6). A similar behavior was observed for L55P-TTR at the same incubation times (L55P-TTR/Ole*A*-*dis*10m and L55P-TTR Ole*A*-*dis*5h in figures 6 g, h and inserts 7,8). These findings suggest that Ole*A* is able to disrupt fibrils favoring the release of oligomer-like species that were substantially devoid of cytotoxicity (see below). All these data nicely agree with previous reports showing that phenols can remodel mature amyloid fibrils to smaller, less-toxic aggregates [22].

3.4. Ole*A* interferes with the interaction of TTR aggregates with the cell membrane

Finally, we sought to investigate whether the presence of Ole*A* affected the cytotoxicity of TTR aggregates grown at pH 4.0 or 5.0. To do this, we treated mouse HL-1 cardiomyocytes for 24 h with 20 μM (monomeric TTR concentration) wt-TTR or L55P-TTR in the absence or in the presence of a threefold excess of Ole*A*. At the end of the incubation the MTT test was used to assay cell viability. No toxic effects were observed in cells treated with Ole*A* only (Fig. 7i, l), whereas wt-TTR and L55P-TTR aggregated for 72 h (wt-TTR-*i*72h) or 96 h (L55P-TTR-*i*96h) were found to be toxic to exposed cells. Cell viability was about 60 ± 6.84% and 50 ± 3.32%, respectively, as compared to that of cells exposed to vehicle or to early aggregates (Fig. 7i, l). However, the aggregates of both proteins grown in the presence of Ole*A* (wt-TTR/Ole*A*-*i*72h and L55P-TTR/Ole*A*-*i*96h) were found to be much less toxic; in fact, at these conditions cell viability was not modified in cells exposed to wt-TTR (wt-TTR/Ole*A*-*i*72h) and only slightly reduced in cells exposed to L55P-TTR (L55P-TTR/Ole*A*-*i*96h).

We also checked whether the fibril disaggregating power of Ole*A* modified the toxicity of wt-TTR-*i*72h or L55P-TTR-*i*96h pre-formed fibrils. To this aim, the fibrils of either protein were incubated in the presence of Ole*A* at a 1:3 monomeric TTR:Ole*A* molar ratio for 10 min (wt-TTR/Ole*A*-*dis*10min and L55P-TTR/Ole*A*-*dis*10min) or for 5 h (wt-TTR/Ole*A*-*dis*5h and L55P-TTR-Ole*A*-*dis*5h) and then added to the cell culture media. Respect to the treatment with pre-formed fibrils, the MTT assay showed an increase of cell viability of about 85 ± 8.5% for wt-TTR/Ole*A*-*dis*10min and of about 95 ± 4.54% for wt-TTR/Ole*A*-*dis*5h (Fig. 7i), and of about 80 ± 5.6% for both L55P-TTR/Ole*A*-dis10min and L55P-TTR-Ole*A*-dis5h samples (Fig. 7l). These data clearly showed that Ole*A* not only modified the structural features of pre-formed amyloid fibrils of both wt-TTR and L55P-TTR, but that these modifications reduced their cytotoxicity. All these data nicely paralleled the cytotoxicity of TTR aggregates; indeed, the latter reached a maximum with 72 h-aged aggregates, which matched the highest extent of solvent-exposure of aromatic residues (Fig. 4) [47].

It has been reported that Ole*A* defense against aggregate toxicity includes some increase of cell resistance against aggregate cytotoxicity by stimulation of cell defenses, notably autophagy [48]. We therefore investigated whether Ole*A*, besides interfering with cytotoxic amyloid aggregation of TTR, was also able to increase cell resistance against the cytotoxicity of preformed TTR aggregates. To do this, we supplemented the cardiomyocytes culture media with Ole*A* before exposure to TTR aggregates. We found that pre-incubation with the polyphenol for up to 24 h did not improve cell ability to resist against aggregate toxicity (Supplementary Fig. 1A). These findings suggested that Ole*A* protection against aggregate cytotoxicity did not result from any stimulation of the cell defenses, as it has been reported for neuronal cells; rather it could have arisen from the

interference of Ole*A* with TTR aggregation reported above or with the association of TTR toxic aggregates with the plasma membrane of the exposed cells. We therefore investigated whether the structural changes induced by Ole*A* in TTR aggregates could have modified the interaction of the latter with the cell membrane, a commonly recognized early event of amyloid cytotoxicity. Confocal microscopy images showed that an association between TTR fibrils (wt-TTR-*i*72h and L55P-TTR-*i*96h) administered to the cell culture media for 24 h and the plasma membrane of HL-1 cells does exist (Fig. 7a, e). Such interaction was suppressed when wt-TTR aggregates were grown for 72 h in the presence of Ole*A* (wt-TTR/Ole*A*-*i*72h) (Fig. 7b). The same effect, yet to a lesser extent, was also observed for L55P-TTR aggregates grown for 96 h in the presence of Ole*A* (L55P-TTR/Ole*A*-*i*96h) (Fig. 7f).

To better investigate the effects of Ole*A* on the interaction between mature TTR fibrils and the cell membrane at the molecular level, we treated for 24 h the HL-1 cells with aggregates of mature wt-TTR or L55P-TTR previously treated for 10 min or for 5.0 h with Ole*A* (wt-TTR/Ole*A*-dis10m and wt-TTR/Ole*A*-dis5h; L55P-TTR/Ole*A*-dis10m and L55P-TTR/Ole*A*-dis10m). We found that aggregate interaction with the cell membrane was not substantially altered when the fibrils were treated with Ole*A* for 10 min (Fig. 7 c, g), whereas a prolonged treatment (5 h) consistently reduced aggregate clusterization onto the cells (Fig. 7 d, h).

3.5. OleA reduces the co-localization between GM1 and TTR aggregates

Once shown that TTR aggregates interact with the plasma membrane of the exposed cells and that this is an early event in fibril cytotoxicity, we checked whether TTR aggregates could affect membrane integrity of the exposed cells. To do this, we imaged the cells treated with aggregates by 3D confocal microscopy; we also used sensitized FRET analysis to assess aggregate interaction with the membrane ganglioside GM1, a well known interaction site of amyloid oligomers/fibrils [49, 50]. We found that both wt-TTR and L55P-TTR aggregates associated with the cell membrane (Fig. 8a,c and 8e,g); however, while the former were found to lay onto surface depressions enclosed by intact plasma membrane segments (Fig. 8a, insets 1,1a), only the latter appeared to be able to cross the cell membrane and reach the cytoplasm (Fig. 8c, insets 3,3a), suggesting a different mode of interaction of the two species with cell membrane components. Sensitized FRET analysis between TTR and GM1 shed light on such a difference. We recorded higher FRET signals in cells treated with aggregated L55P-TTR (Fig. 8g) than in cells treated with aggregated wt-TTR (Fig. 8e). Differently to what expected from the TEM analysis, the HL-1 cells treated with wt-TTR/Ole*A*-*i*72h showed diffuse dots of TTR immunofluorescence (characterized by a low FRET efficiency with GM1) and the absence of amorphous aggregate clusters (Fig. 8b,e). On the contrary, besides diffused staining of fluorescence dots, sporadic clusters of aggregates were observed in the L55P-TTR/Ole*A*-*i*96h sample, that was characterized by a higher FRET efficiency (Fig. 8d, inset 4,8h). Taken together, these data indicate that L55P aggregates interact more consistently than wt-TTR aggregates at GM1-rich sites, in agreement with their higher cytotoxicity and, possibly, with their higher hydrophobic exposure. Our data also support the idea that the aggregates of the two proteins interact with the cell membrane with different strength and partially different consequences in terms of cell viability.

3.6. Ole*A* induces disaggregation of wt- and L55P-TTR fibrils

Finally, we analyzed by FRET/confocal microscopy how preformed aggregates treated with Ole*A* (that proved to induce morphological changes, as shown above) interact with the cell membrane. wt-TTR and L55P-TTR immuno-fluorescent aggregates incubated for 10 min with Ole*A* (wt-TTR/ and L55P-TTR/Ole*A*-*dis*10m) were observed as sparse clusters mixed with diffused immuno-fluorescent dots, both with low FRET signal (Fig. 9a, c and e, g). Interestingly, the number of dots increased with the time of aggregate treatment with Ole*A* for both wt-TTR and L55P-TTR (Fig. 9b, d and 9f, h).

All these data, along with those on aggregate cytotoxicity, morphology and CR binding suggest that the overall effect of Ole*A* may be that of remodeling preformed aggregates to less-toxic, less-ordered, smaller aggregates that maintain their ability to interact with the cell membrane at GM-rich sites, but to a lesser extent and without major effects on membrane integrity.

4. Discussion

Recent studies indicate that several small aromatic compounds interfere with amyloid aggregation, possibly by remodeling the amyloid intermediates through different mechanisms of interactions with the aggregating monomers/intermediates [51, 52]. Studies with cultured cells and model organisms have confirmed such beneficial effects against a number of amyloid diseases; so that some of these compounds have been, and presently are being, assayed in several clinical trials. In particular, dietary polyphenols such as resveratrol, curcumin and epigallocatechin-3-gallate (EGCG) have been shown to inhibit TTR aggregation and aggregate toxicity to cardiomyocytes [53], as confirmed by recent data showing reduction of the left ventricular myocardial mass in patients with cardiac SSA amyloidosis after a 12 month treatment with ECGC [54, 55]. Ole*A* is a polyphenol enriched in the extra virgin olive oil, and several studies have convincingly supported its beneficial effects against age-associated neurodegeneration and other pathologies including type 2 diabetes and, possibly, its protection against toxic cardiomyopathy [56]. However, no evidence has been reported so far on possible beneficial effects of Ole*A* against TTR aggregation and aggregate cytotoxicity, particularly to cardiomyocytes. Here we performed an accurate biophysical study on (i) the modifications of the aggregation path of wt-TTR and one of its more investigated amyloidogenic mutants, L55P; (ii) the effects of Ole*A* on the stability of pre-formed mature fibrils of the two TTR variants; (iii) the biophysical modifications occurring in the two protein variants and their assemblies arising in the aggregation path both in the absence and in the presence of Ole*A*; (iv) the way Ole*A* interferes with the cytotoxicity of the aggregation intermediates and the end products of wt-TTR and L55P-TTR by using a cardiac cell line; (v) the biophysical features underlying aggregate membrane interaction.
Our findings confirmed that L55P-TTR is significantly more toxic than wt-TTR [57]; however, the presence of Ole*A* in the aggregation mixture resulted in the growth of aggregates substantially harmless, confirming the protective power of this polyphenol even for what TTR toxicity to a cardiac cell line is concerned. The loss of

TTR aggregate cytotoxicity is likely related to the poor interaction between the resulting TTR/Ole*A* complexes and GM1 found in the lipid rafts domains of the plasma membrane of the exposed cells (see below).

Our biophysical study, aimed at providing data useful to explain Ole*A* protection against TTR aggregate toxicity, suggests that Ole*A* modifies the aggregation path of TTR favoring the appearance of soluble non-toxic aggregates as well as non-toxic mature fibrils. The FTIR analysis of L55P- and wt-TTR indicates that, for both proteins, misfolding with subsequent aggregation is an irreversible process apparently not affected by Ole*A*. From these observations we suggest that Ole*A* acts by favoring the formation of non-toxic TTR aggregates rather than by protecting TTR from misfolding and subsequent aggregation by structural stabilization. In particular, the CR, FTIR, intrinsic fluorescence and fluorescence quencing data support the idea that a major signature of the inhibition of TTR amyloid polymerization by Ole*A* is the significant decrease of solvent-exposed aromatic residues which become uncovered following tetramer disassembly and misfolding of the resulting monomers/dimers. It cannot be excluded that the latter effect at least in part can also result from a direct interaction of Ole*A* with hydrophobic patches that become exposed during the aggregation reaction, modifying its path and resulting in a sort of shielding, neutralizing effect. Similar considerations also apply to explain both the reduced toxicity of mature fibrils grown in the presence of Ole*A* and the interaction of Ole*A* with pre-formed mature fibrils, resulting in fibril disassembly. The strongly reduced toxicity of these assemblies appear to result from their impaired ability to interact with the cell membrane possibly as a consequence of a reduced hydrophobic exposure following altered conformational features and/or some masking of exposed hydrophobic residues by Ole*A* molecules.

That Ole*A* and TTR do interact is also supported by the analysis of the emission spectra of the aromatic residues, that shows a reduction of the decrease of the 320-330 nm component observed in the second derivative plots during TTR aggregation in the presence of Ole*A*. Of note, the secondary derivative plots of the most toxic species grown from both wt-TTR and L55P-TTR displayed a peculiar minimum around 335 nm a spectral component absent in the less toxic Ole*A*/fibrils complex. Therefore, we suggest that TTR incubation with the polyphenol affects amyloid TTR toxicity by hampering its interaction with other molecules. This conclusion is supported by the acrylamide quenching analysis, which showed some alteration of solvent-exposure of peptide aromatic residues in the presence of Ole*A*. Recent research suggested that aromatic interactions favor molecular recognition of amyloidogenic sequences by enhancing the directionality and orientation needed for the ordered self-assembly process and hence fibril assembly kinetics [58]. On the other hand, it has been reported that several polyphenols are able to interact with amyloidogenic aromatic residues hindering π-system stacking [59, 60], inhibiting the elongation phase of fibril growth or the assembly of large oligomers without interfering with early nucleation events [60]. Modeling studies have shown that several polyphenols share the ability to adopt a specific three-dimensional conformation that might be essential for early amyloid binding preventing the growth of typical amyloid fibrils [61].

Our data extend these findings also to the Ole*A*/TTR system, suggesting that this polyphenol can interfere with TTR fibril assembly and is able to promote mature fibrils disruption. In particular, our TEM analysis revealed

that Ole*A* modifies the fibrillation process increasing the population of both oligomer-like structures and unstructured aggregates. Importantly, the loss of structural uniformity and the presence of oligomer-like structures were observed also following exposure of mature fibrils to Ole*A* suggesting that the latter can induce disruption of both wt- and L55P-TTR fibrils. In view of these data it can be reasonably assumed that the structural modification induced by Ole*A* to aggregated TTR might alter TTR-cell interaction as well as fibril stability in tissue. On this aspect, a recent paper on beta2-microglobulin by the Redford group [62] has shown that minor modifications, such as a shift in pH from 7.4 to 6.4, modifies the molecular shedding of pre-formed fibrils whose disassembly liberates non-toxic native monomers or toxic non-native spherical oligomers, respectively. These data suggest that the endocytic trafficking through acidic compartments may be a key factor in amyloid diseases at least for all those protein/peptides, such as TTR, whose aggregation path is affected by the pH value [62] and that Ole*A* could be beneficial non only by favoring non-toxic fibril disassembly but also avoiding the possible endocytosis-associated toxicity. Moreover oligomers arising from OleA-induced fibril disassembly are unlikely to seed further fibril growth considering recent reports suggesting that TTR fibrils do not induce any increase in fluorescence signal when incubated with newly dissolved TTR [63] and that misfolded TTR monomers efficiently aggregate by a downhill polymerization mechanism and thus, TTR aggregation is not susceptible to seeding [64].

Emerging evidence points to fibrils/membrane interaction as a key factor of the cytotoxic potential of amyloid aggregates [65, 66]. Our confocal analysis supported the latter hypothesis revealing that aggregate-exposed cells displayed a lower affinity to Ole*A*-treated than to Ole*A*-untreated TTR samples. Moreover, TEM results were confirmed by a diffuse FRET signal in cells exposed to Ole*A*-treated aggregates indicating the presence of oligomer-like structures on their plasma membranes. In addition, the low efficiency of FRET signal between TTR and GM1 recorded in exposed cells allows to relate the cytoprotective effect of Ole*A* to a decreased interaction between the Ole*A*/TTR complex and the plasma membrane at GM1-enriched sites found in ordered membrane domains, most often referred to as lipid rafts. On this aspect, it must be reminded that previous data have highlighted the importance of negative charges carried by anionic phospholipids (but also by GM1) [64] as well as of hydrophobic exposure [67] for TTR binding to the cell membrane.

In conclusion, our results indicate that Ole*A* reduces amyloid TTR toxicity, specifically to a cardiac cell line. Previous data on the protection given by resveratrol, another natural polyphenol, and its analogs against cardiomyocyte toxicity by TTR have shown a mechanism related to TTR stabilization [52]. Our study indicates that Ole*A* protection results from a different mechanism whereby its interaction with TTR does not stabilize the tetramer or it hinders TTR transition to an amyloid structure which interacts with the cell membrane altering its structural features. Rather, Ole*A* interferes with TTR fibrillation by stabilizing an oligomer-like intermediate that interacts with the plasma membrane without altering its integrity. Alterations of membrane fluidity resulting from TTR interaction with neuronal cells, with subsequent modification of membrane permeability, were previously reported to be a key event in protein cytotoxicity [68]. Importantly, Ole*A* is also able to disassemble pre-formed TTR mature fibrils into the same non-toxic oligomer-like intermediates. These data suggest that

Ole*A*, or its molecular scaffold can be a good starting point to design novel molecules useful for prevention and therapy of TTR-associated sporadic or familial amyloidosis. Although current polyphenol researches have limited impact on clinical practice, they have strong evidence and testable hypothesis to contribute clinical advances and drug discovery towards TTR-associated amyloidosis. Therefore, future studies focusing on human clinical trials of different polyphenols that interfere in different ways with TTR aggregation (e.g. OleA and EGCG) and on their combinations, with potential synergistic effects, should be carried out. These future researches will be useful to understand the usefulness to combine the administration of different anti-amyloidogenic compounds and will likely provide the base for a new generation of phytopharmaceuticals.

ACKNOWLEDGMENTS: This project was supported by Italian MIUR, PRIN 2009 (2009KN2FBM_002). M.L. was supported by grant from Ente Cassa di Risparmio di Firenze (N° 2013.0697); M.R. was supported by the Italian Ministry for Education University and Research (MIUR) framework "Futuro in Ricerca 2010" (N° RBFR109EOS).

References

[1] Blake CC, Geisow MJ, Swan IDA. Structure of human plasma prealbumin at 2-5 A resolution. A preliminary report on the polypeptide chain conformation, quaternary structure and thyroxine binding. J. Mol. Biol. 1974; 88:1–12.

[2] Dickson PW, Aldred AR, Marley PD, Tu GF, Howlett GJ, Schreiber G. High prealbumin and transferrin mRNA levels in the choroid plexus of rat brain. Biochem. Biophys. Res. Commun. 1985; 127:890–5.

[3] Noy N, Slosberg E, Scarlata S. Interactions of retinol with binding proteins: studies with retinol-binding protein and with transthyretin. Biochemistry 1992;31:11118–24.

[4] Sekijima Y, Kelly JW, Ikeda S. Pathogenesis of and therapeutic strategies to ameliorate the transthyretin amyloidoses. Curr. Pharm. Des. 2008;14:3219–30.

[5] Cornwell GGIII, Murdoch WL, Kyle RA, Westermark P, Pitkanen P. Frequency and distribution of senile cardiovascular amyloid. A clinicopathologic correlation. Am. J. Med. 1983;75:618–23.

[6] Westermark P, Sletten K, Johansson B, Cornwell GGIII. Fibril in senile systemic amyloidosis is derived from normal transthyretin. Proc. Natl. Acad. Sci.USA 1990;87:2843–45.

[7] Connors LH, Lim A, Prokaeva T, Roskens VA, Costello CE. Tabulation of human transthyretin (TTR) variants 2003. Amyloid 2003;10:160–84.

[8] Soares ML, Coelho T, Sousa A, Holmgren G, Saraiva MJ, Kastner DL et al. Haplotypes and DNA sequence variation within and surrounding the transthyretin gene: genotype-phenotype correlations in familial amyloid polyneuropathy (V30M) in Portugal and Sweden. Eur. J. Hum. Genet. 2004; 12:225-37.

[9] Keetch CA, Bromley EH, McCammon MG, Wang N, Christodoulou J, Robinson CV. L55P transthyretin accelerates subunit exchange and leads to rapid formation of hybrid tetramers. J. Biol. Chem. 2005;280:41667-74.

[10] Reixach N, Deechongkit S, Jiang X, Kelly JW, Buxbaum JN. Tissue damage in the amyloidoses: transthyretin monomers and nonnative oligomers are the major cytotoxic species in tissue culture. Proc. Natl. Acad. Sci. USA 2004;101:2817−22.

[11] Hammarstrom P, Wiseman RL, Powers ET, Kelly JW. Prevention of transthyretin amyloid disease by changing protein misfolding energetics. Science 2003;299:713−16.

[12] Obici L, Merlini G. An overview of drugs currently under investigation for the treatment of transthyretin-related hereditary amyloidosis. Expert. Opin. Investig. Drugs 2014;23:1239-51

[13] Stefani M, Rigacci S. Beneficial properties of natural phenols: Highlight on protection against pathological conditions associated with amyloid aggregation. Biofactors 2014;40:482-93.

[14] Queen BL, Tollefsbol TO. Polyphenols and aging. Curr. Aging. Sci. 2010;3:34–42.

[15] Scarmeas NY, Stern MX, Tang R, Mayeux JA, Luchsinger JA. Mediterranean diet and risk for Alzheimer's disease. Ann. Neurol. 2006;59:912–21.

[16] Feart C, Samieri C, Barberger-Gateau P. Mediterranean diet and cognitive function in older adults. Curr. Opin. Clin. Nutr. Metab. Care. 2010;13:14–18.

[17] Rigacci S, Guidotti V, Bucciantini M, Parri M, Nediani C, Cerbai E et al. Oleuropein aglycon prevents cytotoxic amyloid aggregation of human amylin. J. Nutr. Biochem. 2010;21:726–735.

[18] Rigacci S, Guidotti V, Bucciantini M, Nichino D, Relini A, Berti A et al. Aβ(1–42) aggregates into non-toxic amyloid assemblies in the presence of the natural polyphenol Oleuropein aglycon. Curr. Alzheimer. Res. 2011;8:841–52.

[19] Daccache A, Lion C, Sibille N, Gerard M, Slomianny C, Lippens G et al. Oleuropein and derivatives from olives as Tau aggregation inhibitors. Neurochem. Int. 2011;58:700-7.

[20] Diomede L, Rigacci S, Romeo M, Stefani M, Salmona M. Oleuropein aglycone protects transgenic C. elegans strains expressing Aβ42 by reducing plaque load and motor deficit. PLoS One 2013;8:e58893.

[21] Luccarini I, Grossi C, Rigacci S, Coppi E, Pugliese AM, Pantano D et al. Oleuropein aglycone protects against pyroglutamylated-3 amyloid-ß toxicity: biochemical, epigenetic and functional correlates. Neurobiol. Aging 2015;36:648-63

[22] Ladiwala AR, Dordick JS, Tessier PM. Aromatic small molecules remodel toxic soluble oligomers of amyloid beta through three independent pathways. J. Biol. Chem. 2011;286:3209-18.

[23] Miyata M, Sato T, Kugimiya M, Sho M, Nakamura T, Ikemizu S et al. The crystal structure of the green tea polyphenol (−)-epigallocatechin gallate-transthyretin complex reveals a novel binding site distinct from the thyroxine binding site. Biochemistry 2010;49:6104–14.
[24] Ferreira N, Santos SA, Domingues MR, Saraiva MJ, Almeida MR. Dietary curcumin counteracts extracellular transthyretin deposition: Insights on the mechanism of amyloid inhibition. Biochim. Biophys. Acta 2013;1832:39–45.
[25] Ferreira N, Saraiva MJ, Almeida MR. Natural polyphenols inhibit different steps of the process of transthyretin (TTR) amyloid fibril formation. FEBS Lett. 2011;585:2424–30.
[26] White SM, Constantin PE, Claycomb WE. Cardiac physiology at the cellular level: use of cultured HL-1 cardiomyocytes for studies of cardiac muscle cell structure and function. Am. J. Physiol. Heart Circ. Physiol. 2004;286:H823–29.
[27] Mangione PP, Porcari R, Gillmore JD, Pucci P, Monti M, Porcari M et al. Proteolytic cleavage of Ser52Pro variant transthyretin triggers its amyloid fibrillogenesis. Proc. Natl. Acad. Sci. U S A 2014;111:1539-44.
[28] Bonifacio MJ, Sakaki Y, Saraiva MJ. "In vitro" amyloid fibril formation from transthyretin: The influence of ions and the amyloidogenicity of TTR variants. Biochim. Biophys. Acta 1996;1316:35– 42.
[29] Nilsson MR. Techniques to study amyloid fibril formation in vitro. Methods 2004;34:151-60.
[30] Frid P, Anisimov SV, Popovic N. Congo red and protein aggregation in neurodegenerative diseases. Brain Res. Rev. 2007;53:135-60.
[31] Sartiani L, Bochet P, Cerbai E, Mugelli A, Fischmeister R. Functional expression of the hyperpolarization-activated, non-selective cation current I(f) in immortalized HL-1 cardiomyocytes. J Physiol 2002;545:81-92.
[32] Nosi D, Mercatelli R, Chellini F, Soria S, Pini A, Formigli L et al. A molecular imaging analysis of Cx43 association with Cdo during skeletal myoblast differentiation. J. Biophotonics 2012;6:612-61.
[33] Natalello A, Ami D, Doglia SM Fourier transform infrared spectroscopy of intrinsically disordered proteins: measurement procedures and data analyses. Methods Mol. Biol. 2012;895:229-44.
[34] Ami D, Ricagno S, Bolognesi M, Bellotti V, Doglia SM, Natalello A. Structure, stability, and aggregation of β-2 microglobulin mutants: insights from a Fourier transform infrared study in solution and in the crystalline state. Biophys J 2012;102:1676-84.
[35] Susi H, Byler DM. Resolution-enhanced Fourier transform infrared spectroscopy of enzymes. Methods Enzymol. 1986;130:290-311.
[36] Kumar V, Sharma VK, Kalonia DS. Second derivative tryptophan fluorescence spectroscopy as a tool to characterize partially unfolded intermediates of proteins. Int. J. Pharm. 2005;294:193-9.
[37] Souillac PO, Uversky VN, Fink AL. Structural Transformations of Oligomeric Intermediates in the Fibrillation of the Immunoglobulin Light Chain LEN. Biochemistry 2003;42:8094–104.
[38] Pitozzi V, Jacomelli M, Zaid M, Luceri C, Bigagli E, Lodovici M et al. Effects of dietary extra-virgin olive oil on behaviour and brain biochemical parameters in ageing rats. Br J Nutr 2010;11:1674–1683.
[39] Farr SA, Price TO, Dominguez LJ, Motisi A, Saiano F, Niehoff ML et al. Extra virgin olive oil improves learning and memory in SAMP8 mice. J. Alzheimers Dis. 2012;28:81–92.
[40] Shen Y, Song SJ, Keum N, Park T. Olive leaf extract attenuates obesity in high-fat diet-fed mice by modulating the expression of molecules involved in adipogenesis and thermogenesis. Evid Based Complement Alternat Med. 2012;2014:971890.
[41] Omar SH Cardioprotective and neuroprotective roles of Oleuropein in olive. Saudi Pharm. J. 2010;18:111-121.
[42] Lai Z, Colón W, Kelly JW. The acid-mediated denaturation pathway of transthyretin yields a conformational intermediate that can self-assemble into amyloid. Biochemistry 1996;35:6470-82.
[43] Pires RH, Karsai Á, Saraiva MJ, Damas AM, Kellermayer MS. Distinct Annular Oligomers Captured along the Assembly and Disassembly Pathways of TransthyretinAmyloid Protofibrils. PLoS One 2012;7:e44992.
[44] Cordeiro Y, Kraineva J, Suarez MC, Tempesta AG, Kelly JW, Silva JL et al. Fourier transform infrared spectroscopy provides a fingerprint for the tetramer and for the aggregates of transthyretin. Biophys. J. 2006;91:957-67.

[45] Zandomeneghi G, Krebs MR, McCammon MG, Fändrich M. FT-IR reveals structural differences between native beta-sheet proteins and amyloid fibrils. Protein Sci. 2004;13:3314-21.
[46] Tallmadge DH, Huebner JS, Borkman RF.Acrylamide quenching of tryptophan photochemistry and photophysics. Photoche. Photobiol. 1989;49:381-6.
[47] Mannini B, Mulvihill E, Sgromo C, Cascella R, Khodarahmi R, Ramazzotti M et al. Toxicity of protein oligomers is rationalized by a function combining size and surface hydrophobicity. ACS Chem. Biol. 2014;9:2309-17.
[48] Grossi C, Rigacci S, Ambrosini S, Ed Dami T, Luccarini I, Traini C et al. The polyphenol Oleuropein aglycone protects TgCRND8 mice against Aß plaque pathology. PLoS One 2013;8:e71702.
[49] Bucciantini M, Nosi D, Forzan M, Russo E, Calamai M, Pieri L et al. Toxic effects of amyloid fibrils on cell membranes: the importance of ganglioside GM1. FASEB J 2012;262:818-31.
[50] Matsuzaki K. How do membranes initiate Alzheimer's Disease? Formation of toxic amyloid fibrils by the amyloid β-protein on ganglioside clusters. Acc Chem Res 2014;478:2397-404.
[51] Bastianetto S, Quirion R. Natural antioxidants and neurodegenerative diseases. Front. Biosci. 2004;9:3447–52.
[52] Pawar AP, Dubay KF, Zurdo J, Chiti F, Vendruscolo M, Dobson CM. Prediction of "aggregation-prone" and "aggregation-susceptible" regions in proteins associated with neurodegenerative diseases. J. Mol. Biol. 2005;350:379–92.
[53] Bourgault S, Choi S, Buxbaum JN, Kelly JW, Price JL, Reixach N. Mechanisms of transthyretin cardiomyocyte toxicity inhibition by resveratrol analogs. Biochem. Biophys. Res. Commun. 2011;410:707-13.
[54] Kristen AV, Lehrke S, Buss S, Mereles D, Steen H, Ehlermann P et al. Green tea halts progression of cardiac transthyretin amyloidosis: an observational report. Clin Res Cardiol. 2012;101:805-13.
[55] aus dem Siepen F, Buss SJ, Andre F, Seitz S, Giannitsis E, Steen H, et al. Extracellular remodeling in patients with wild-type amyloidosis consuming epigallocatechin-3-gallate: preliminary results of T1 mapping by cardiac magnetic resonance imaging in a small single center study. Clin Res Cardiol. 2015;104:640-7.
[56] Andreadou I, Mikros E, Ioannidis K, Sigala F, Naka K, Kostidis S et al. Oleuropein prevents doxorubicin-induced cardiomyopathy interfering with signaling molecules and cardiomyocyte metabolism. J. Mol. Cell Cardiol. 2014;69:4-16.
[57] Yang M, Lei M, Huo S. Why is Leu55 → Pro55 transthyretin variant the mostamyloidogenic: Insights from molecular dynamics simulations of transthyretin monomers. Protein Sci. 2003;12:1222-31.
[58] Porat Y, Mazor Y, Efrat S, Gazit E. Inhibition of islet amyloid polypeptide fibril formation: a potential role for heteroaromatic interactions. Biochemistry 2004;43:14454–62.
[59] Wu C, Lei H, Wang Z, Zhang W, Duan Y. Phenol Red Interacts with the Protofibril-Like Oligomers of an Amyloidogenic Hexapeptide NFGAIL through Both Hydrophobic and Aromatic Contacts. Biophys. J. 2006;91:3664-72.
[60] Gazit E. A possible role for π-stacking in self-assembly of amyloid fibrils. FASEB J. 2002;16:77–83.
[61] Porat Y, Abramowitz A, Gazit E. Inhibition of Amyloid Fibril Formation by Polyphenols: Structural Similarity and Aromatic Interactions as a Common Inhibition Mechanism. Chem. Biol. Drug Des. 2006;67:27–37.
[62] Tipping KW, Karamanos TK, Jakhria T, Iadanza MG, Goodchild SC, Tuma R et al. pH-induced molecular shedding drives the formation of amyloid fibril-derived oligomers. PNAS 2015;112:5691-696.
[63] Westermark G, Westermark P. Transthyretin and Amyloid in the Islets of Langerhans in Type-2 Diabetes. Exp Diabetes Res. 2008;2008:429274.
[64] Eisele YS, Monteiro C, Fearns C, Encalada SE, Wiseman RL, Powers ET et al. Targeting protein aggregation for the treatment of degenerative diseases. Nat Rev Drug Discov. 2015;14:759-80.
[65] Hou X, Richardson SJ, Aguilar MI, Small DH. Binding of amyloidogenic transthyretin to the plasma membrane alters membrane fluidity and induces neurotoxicity. Biochemistry 2005;44:11618-27.
[66] Pieri L, Madiona K, Bousset L, Melki R. Fibrillar α-synuclein and huntingtin exon 1 assemblies are toxic to the cells. Biophys. J. 2012;102:2894-905.

[67] Hong S, Ostaszewski BL, Yang T, O'Malley TT, Jin M, Yanagisawa K et al. Soluble Aβ oligomers are rapidly sequestered from brain ISF in vivo and bind GM1 ganglioside on cellular membranes. Neuron 2014;82:308-319.
[68] Hou X, Mechler A, Martin LL, Aguilar MI, Small DH. Cholesterol and anionic phospholipids increase the binding of amyloidogenic transthyretin to lipid membranes. Biochim. Biophys. Acta 2008;1778:198-205.

Figure Legends

Figure 1. Outline of the chemical structure of Ole*A* (a) and its therapeutic effects (b).

Figure 2. Congo red and DLS analysis of wt- and L55P-TTR aggregation in the presence and in the absence of Ole*A*. Plot of the absorbance ratio at 480/540nm(CR unbound/bound) of wt-TTR (a) and L55P-TTR (c) in native or amyloidogenic conditions in the presence or in the absence of Ole*A*. Absorbance ratio 480/540nm of mature fibrils of wt-TTR (b) and L55P-TTR (d) treated with Ole*A* for 10 min or 5 h. DLS of wt-TTR (e) and L55P-TTR (g) in native or amyloidogenic conditions in the presence or in the absence of Ole*A*. Pre-formed fibrils of wt-TTR (f) or L55P-TTR (h) were treated with Ole*A* for 10 min or 5 h. (i, l) Tables of apparent hydrodynamic diameter of the samples analyzed by DLS.

Figure 3. FT-IR characterization of wt- and L55P-TTR. (a, g) Second derivative FTIR spectra of wt-TTR and L55P-TTR at pH 7.0 recorded at different times of incubation, up to 72 h, and 96h at 37°C. Band assignments to protein secondary structures are indicated. (b, h) Second derivatives of the absorption spectra of wt- and L55P- TTR at pH 7.0 recorded during heating from 37 °C to 100 °C and after sample cooling to 37 °C. (c, i) Second derivative FTIR spectra of wt- and L55P- TTR at pH 3.5 and pH 5.0, respectively, recorded at different incubation times, up to 72 h and 96h at 37°C. (d, l) Second derivatives of the absorption spectra of wt- and L55P- TTR at acid pH recorded during heating from 37 °C to 100 °C, and after sample cooling to 37 °C. (e, m) Second derivative spectra of wt- and L55P- TTR at acid pH in the presence of Ole*A*. The spectra were collected at different incubation times at 37 °C. (f, n) Second derivatives of the absorption spectra of wt- and L55P- TTR at acid pH in the presence of Ole*A* recorded during sample heating from 37 °C to 100 °C, and after cooling to 37 °C. The arrows point to the increasing incubation times (c, e and i,m) or temperature (b,d,f and h, i, n).

Figure 4. Effect of Ole*A* on TTR fluorescence emission. Intrinsic fluorescence emission spectra of wt-TTR (a) and L55P-TTR (f), either alone and in the presence of Ole*A* (b and g) recorded at different times of acid aggregation. The spectra were normalized to fluorescence intensity of 1.0 at λmax, λexc = 295 nm. (d, i) Time point comparison of second derivatives obtained from the emission spectra reported in a-b and f-g. The arrows point to the spectral changes occurring at increasing incubation times. Intrinsic fluorescence emission spectra of wt-TTR (c) and L55P-TTR (h) preformed fibrils treated with Ole*A* for 10 min or 5 h and the relative second derivatives (e, l).

Figure 5. Ole*A* affects surface contacts of TTR amyloid assemblies. Acrylamide quenching of tryptophan fluorescence of wt-TTR (a) and L55P (d) at increasing times of aggregation. Proteins were incubated in the aggregation medium in the absence (a,d) or in the presence (b,e) of Ole*A*. Preformed fibrils of wt-TTR (c) and L55P-TTR (f) treated with Ole*A* for 10 min and 5 h.

Figure 6. Ultra-structural analysis of TTR amyloid assemblies. TEM micrographs of wt-TTR and L55P-TTR, not treated (a, b) or treated with Ole*A* (c, d) at 72 h and 96 h of acid aggregation, respectively. Details of the corresponding selected ROIs showing oligomer-like structures either inside the aggregates (Inserts 1-4) or dispersed on the formvar surface. Pre-formed wt-TTR (e, f) and L55P-TTR (g, h) fibrils treated with Ole*A* for 10 min (e, g) or for 5 h (f, h). Higher magnifications of the corresponding selected ROIs showing dispersed oligomer-like structures (Inserts 5-8). Bars: a-h = 1.0 μm, insert 1 = 120 nm, inserts 2-8 = 60 nm.

Figure 7. Ole*A* affects fibril clustering onto HL-1 cells and on TTR-induced cytotoxicity. Confocal Z-projections of HL-1 cells exposed to wt-TTR or to L55P-TTR fibrils (blue) stained to reveal GM1 (magenta). (a) wt-TTR fibrils and (e) L55P-TTR fibrils grown in aggregation medium for 72 h and 96 h, respectively; (b) wt-TTR/Ole*A*-*i*fibrils and (f) L55P-TTR/Ole*A*-*i*; (c) wt-TTR/OleA-*dis*10m and (g) L55P-TTR/OleA-*dis*10m; (d) wt-TTR/Ole*A*-*dis*5h and (h) L55P-TTR/Ole*A*-*dis*5h.The HL-1 cells were treated for 24 h with 20 μM wt-TTR (i) or L55P-TTR (l) at different times of aggregation or with their pre-formed fibrils in the absence or in the presence of Ole*A* (1:3 ratio). Cell viability was assessed by the MTT reduction assay. Error bars indicate the standard deviation of independent experiments carried out in triplicate. (i) $F_{8,18} = 38,8$; * $p < 0.01$ vs control (5); ° $p < 0.01$ vs wt-TTR/OleA-*i* 72h. (l) $F_{8,18} = 34,3$; * $p < 0.01$ vs control; ° $p < 0.01$ vs L55P-TTR/OleA-i 96h.

Figure 8. 3D and FRET confocal analysis of fibrils interaction with the plasma membrane of HL-1 cells. (a,b) Z-projection of wt-TTR (a) and wt-TTR/OleA-i72h (b) immunostaining (blue) and GM1

staining (magenta) on the HL-1 cell membrane; (1 1a) 3D-volume renderings of regions selected in A showing details of the cell surface (1) and the cytoplasmic area (1a) obtained by performing a volume crop on z-axis. (e and f) Analysis of FRET between GM1 staining and fibril immunostaining; FRET (yellow) and 543 nm laser (blue) excited fibril immunofluorescence, FRET efficiency is shown in 5 and 6. (c, d) L55P-TTR (c) and L55P-TTR/Ole*A*-*i*fibrils (d) on HL-1 cells. (3 and 3a) 3D-volume renderings of the corresponding selected regions; TTR aggregates on the cell surface are indicated by arrows in 3a. (g, h) FRET analysis between GM1 staining and fibrils immunostaining; FRET efficiency is shown in 7 and 8.

Figure 9. Fibril treatment with Ole*A* affects fibril-membrane interaction. (a) Z-projection of wt-TTR/Ole*A*-*dis*10m fibril immunostaining (blue) and GM1 (magenta) on HL-1 cell plasma membrane; (insets 1 and 1a) 3D-volume renderings of corresponding selected regions showing increasing magnifications of TTR aggregates interacting with GM1 on the cell surface. (band inset 2) Analysis of FRET between GM1 staining and fibril immunostaining; FRET (yellow) and 543 nm laser (blue) excited fibril immunofluorescence are shown in (b), FRET efficiency is shown in inset 2. (c) wt-TTR/Ole*A*-*dis*5h fibrils on HL-1 cells. (insets 3 and 3a) 3D-volume renderings of regions selected in C showing amyloid aggregates interacting with GM1 on the cell surface (3); dots of TTR aggregates on the cell surface are indicated by arrows in 3a. (d) FRET analysis between GM1 staining and wt-TTR/Ole*A*-*dis*5h fibrils immunostaining; FRET efficiency is shown in inset 4. (e and insets 5 and 5a) L55P-TTR/Ole*A*-*dis*10m fibrils on HL-1cells. (5 and 5a) 3D-volume renderings of the selected regions showing details of the cell surface; the arrows indicate diffused TTR aggregates on the cell surface. (f) FRET analysis between GM1 staining and L55P-TTR/Ole*A*-*dis*10mfibrils immunostaining; FRET efficiency is shown in 6. (g) L55P-TTR/Ole*A*-*dis*5h fibrils on HL-1cells; (7 and 7a) 3D-volume renderings of selected regions showing details of the cell surface; the arrows indicate diffused TTR aggregates on the cell surface. (h) FRET analysis between GM1 staining and L55P-TTR/Ole*A*-*dis*5h fibrils immunostaining; FRET efficiency is shown in 8.

Supplementary Figure 1. Pre-treatment of HL-1 with Ole*A* and confocal control. a) HL-1 pre-treated with Ole*A* for 24h before the treatment with 20 μM TTR aggregates. Cell viability was assessed by the MTT reduction assay. Error bars indicate the standard deviation of independent experiments carried out in triplicate t-student analysis: * $p<0.005$; ** $p<0.001$; *** $p<0.0001$. b) Confocal images with native TTR immunostaining (blue) and GM1 (magenta) on HL-1 cell plasma membrane.

Figure1

Click here to download high resolution image

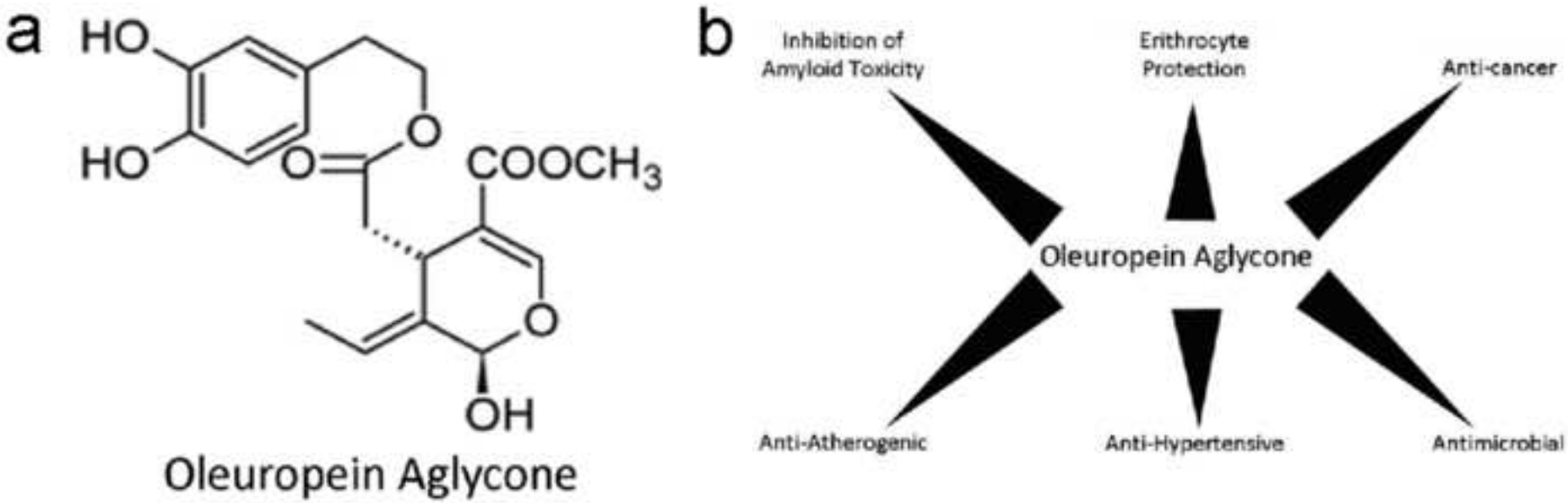

Figure2

Click here to download high resolution image

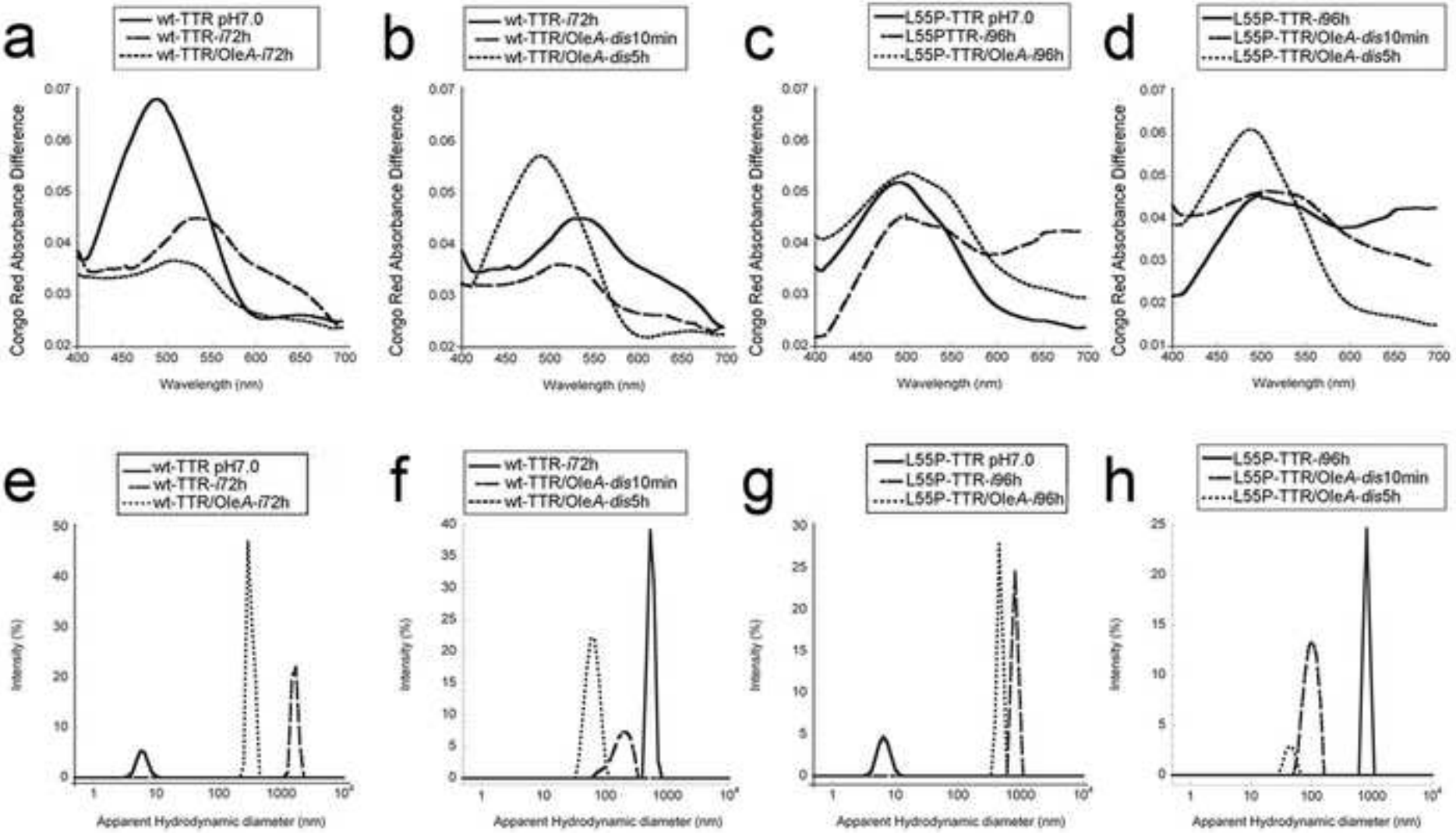

i

	Apparent Hydrodynamic Diameter (nm)
wt-TTR pH7.0	6.9 ± 0.22
wt-TTR-*i*72h	1181.7
wt-TTR/OleA-*i*72h	327.85
wt-TTR/OleA-*dis*10min	141.77
wt-TTR/OleA-*dis*5h	68.061

l

	Apparent Hydrodynamic Diameter (nm)
L55P-TTR pH7.0	6.6±0.30
L55P-TTR-*i*96h	1295.5
L55P-TTR/OleA-*i*96h	511.9
L55P-TTR/OleA-*dis*10min	105.71
L55P-TTR/OleA-*dis*5h	43.821

Figure3

Click here to download high resolution image

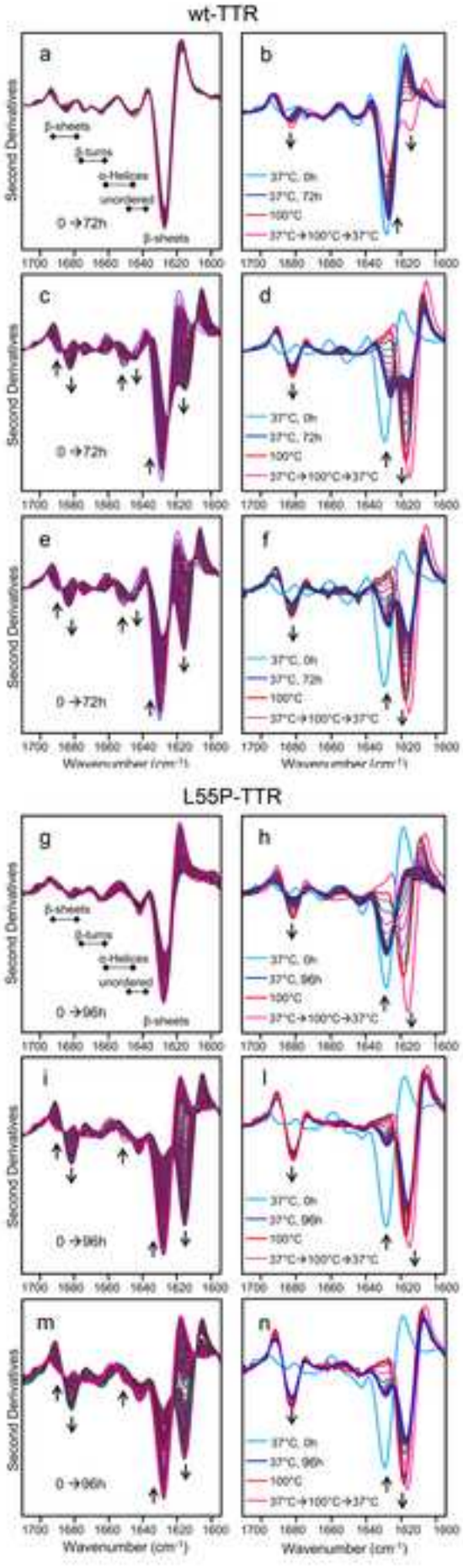

Figure4

Click here to download high resolution image

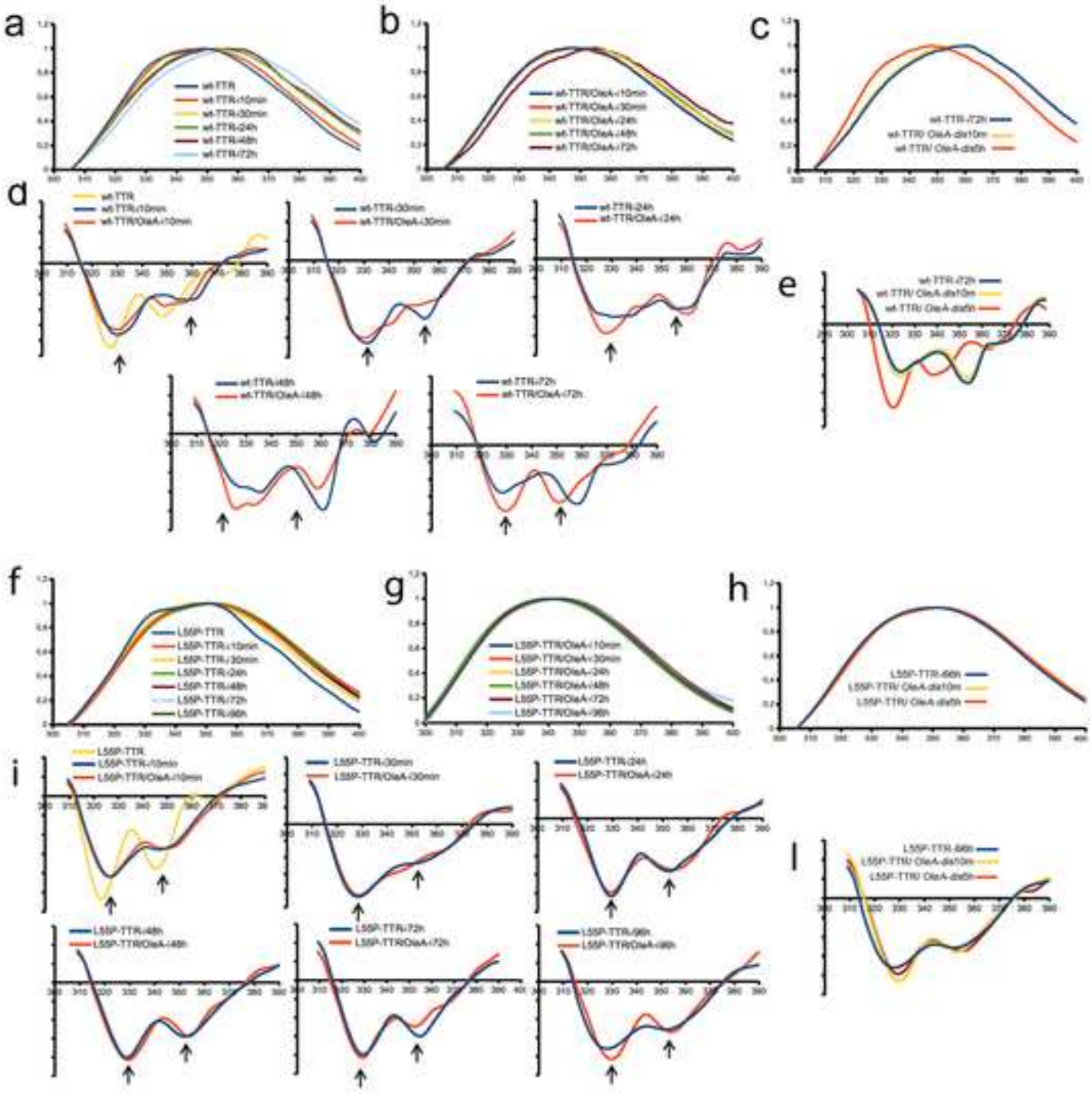

Figure5

Click here to download high resolution image

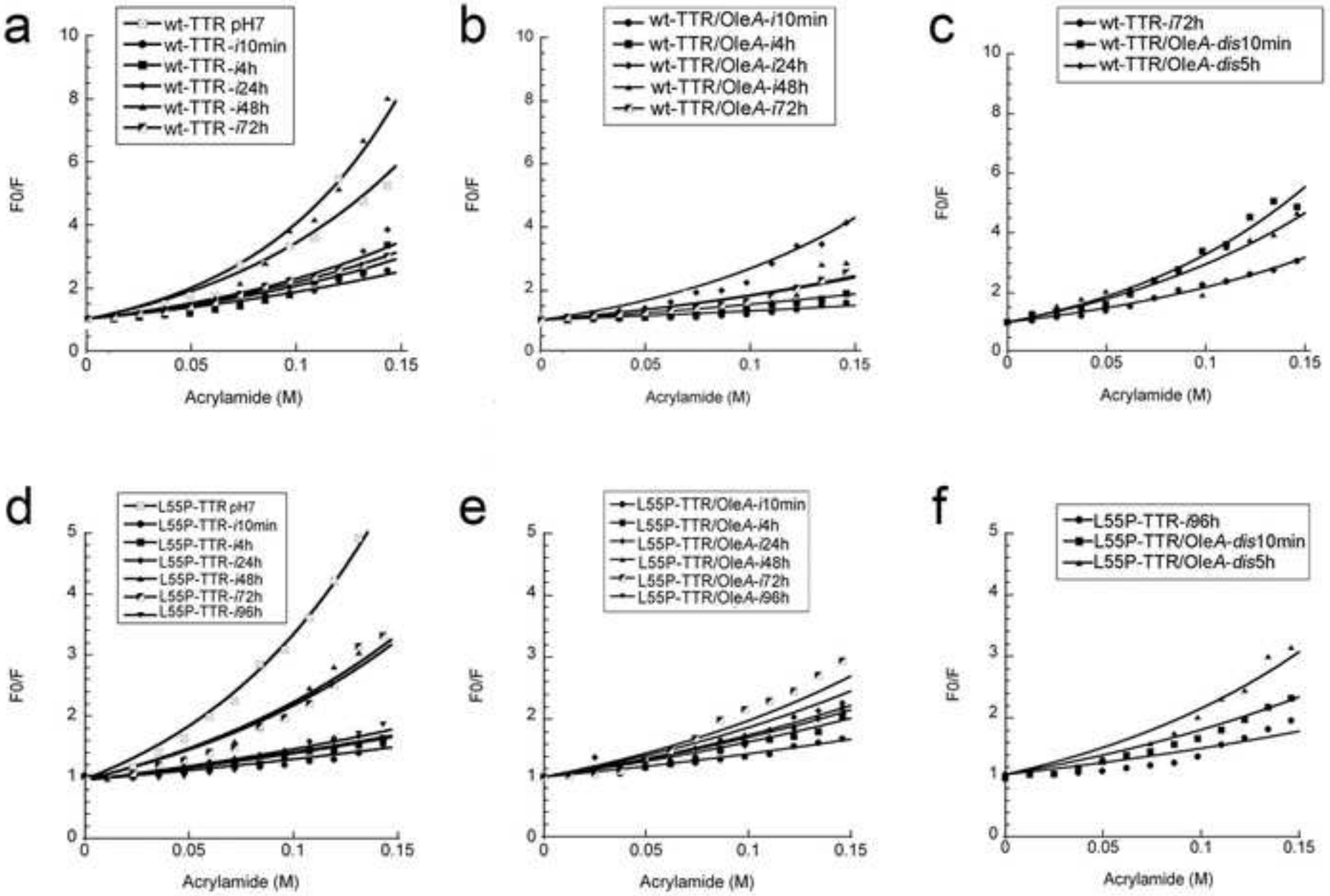

Figure6

Click here to download high resolution image

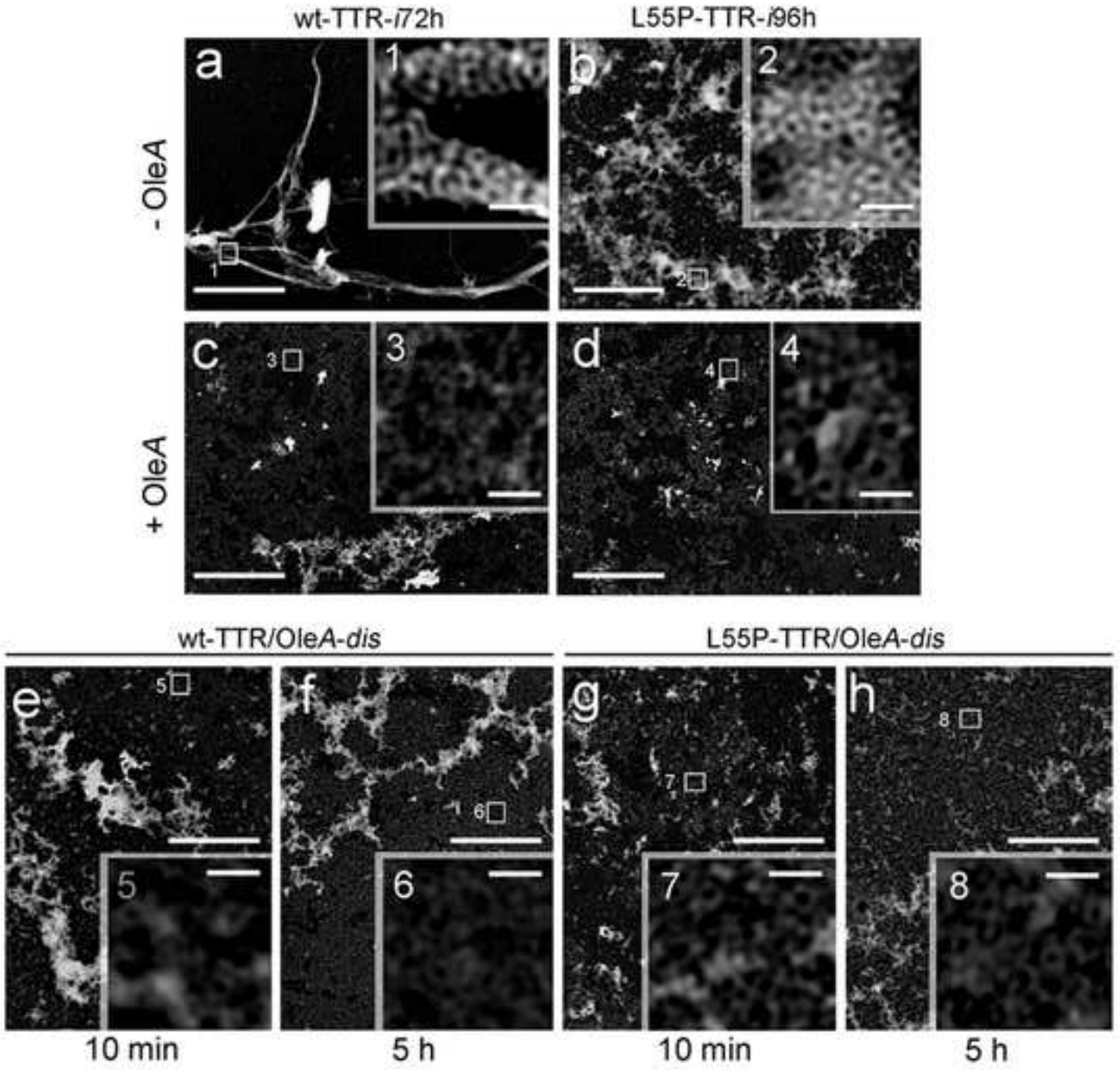

Figure7

Click here to download high resolution image

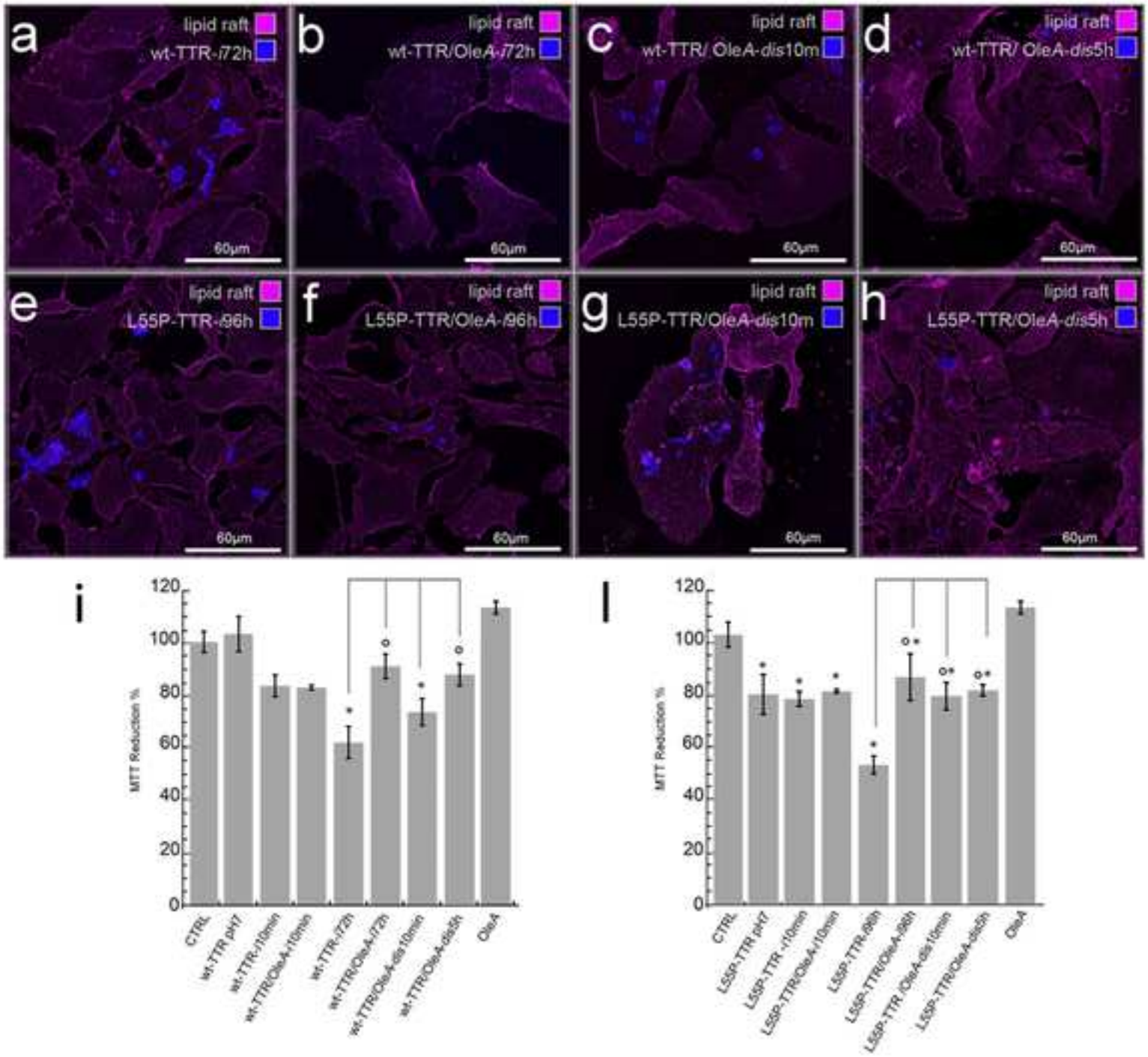

Figure8

Click here to download high resolution image

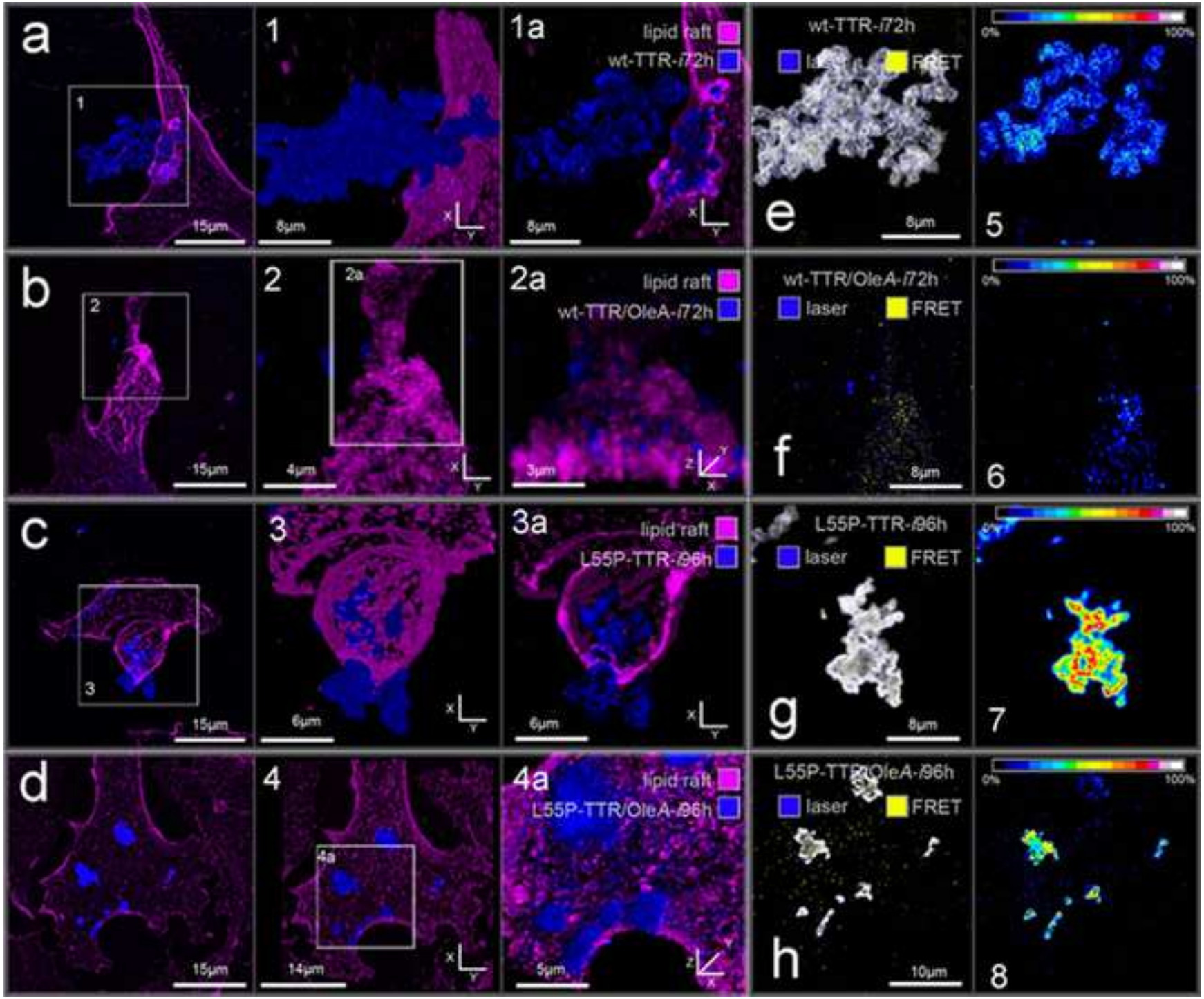

Figure9

Click here to download high resolution image

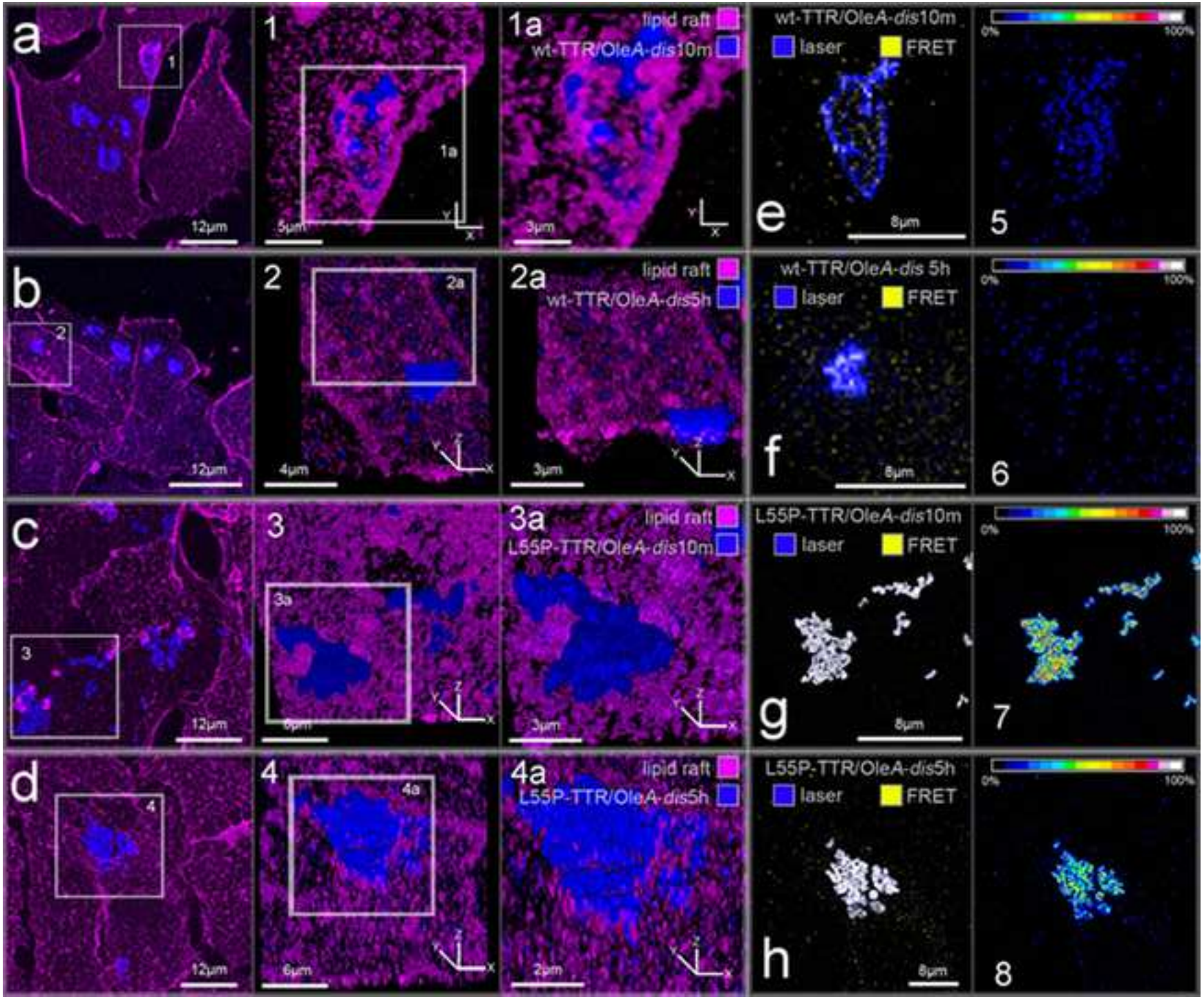

Supplemental file for online publication

Click here to download Supplemental file for online publication: SUPPLEMENTARY1.tif